Inorg. Chem. **2005**, *44*, 7717–7731

Kinetic and Mechanistic Studies on the Reaction of Nitric Oxide with a Water-Soluble Octa-anionic Iron(III) Porphyrin Complex

Joo-Eun Jee,[†] Siegfried Eigler,[§] Frank Hampel,[§] Norbert Jux,*[,§] Maria Wolak,[†,‡] Achim Zahl,[†] Grazyna Stochel,[‡] and Rudi van Eldik*[,†]

Institute for Inorganic Chemistry, University of Erlangen−Nürnberg, Egerlandstrasse 1, 91058 Erlangen, Germany, Institute for Organic Chemistry, University of Erlangen−Nürnberg, Henkestrasse 42, 91054 Erlangen, Germany, and Department of Inorganic Chemistry, Jagiellonian University, Ingardena 3, 30-060 Krakow, Poland

Received June 8, 2005

The polyanionic water-soluble and non-μ-oxo-dimer-forming iron porphyrin iron(III) 5^4,10^4,15^4,20^4-tetra-*tert*-butyl-5^2,5^6,15^2,15^6-tetrakis[2,2-bis(carboxylato)ethyl]-5,10,15,20-tetraphenylporphyrin, $(P^{8-})Fe^{III}$ (**1**), was synthesized as an octasodium salt by applying well-established porphyrin and organic chemistry procedures to bromomethylated precursor porphyrins and characterized by standard techniques such as UV–vis and ^{1}H NMR spectroscopy. A single pK_{a1} value of 9.26 was determined for the deprotonation of coordinated water in $(P^{8-})Fe^{III}(H_2O)_2$ (**1-H$_2$O**) present in aqueous solution at pH <9. The porphyrin complex reversibly binds NO in aqueous solution to give the mononitrosyl adduct, $(P^{8-})Fe^{II}(NO^+)(L)$, where L = H_2O or OH^-. The kinetics of the binding and release of NO was studied as a function of pH, temperature, and pressure by stopped-flow and laser flash photolysis techniques. The diaqua-ligated form of the porphyrin complex binds and releases NO according to a dissociative interchange mechanism based on the positive values of the activation parameters $\Delta S^{\ddagger}$ and $\Delta V^{\ddagger}$ for the "on" and "off" reactions. The rate constant $k_{on} = 6.2 \times 10^4$ M^{-1} s^{-1} (24 °C), determined for NO binding to the monohydroxo-ligated $(P^{8-})Fe^{III}(OH)$ (**1-OH**) present in solution at pH >9, is markedly lower than the corresponding value measured for **1-H$_2$O** at lower pH ($k_{on} = 8.2 \times 10^5$ M^{-1} s^{-1}, 24 °C, pH 7). The observed decrease in the reactivity is contradictory to that expected for the diaqua- and monohydroxo-ligated forms of the iron(III) complex and is accounted for in terms of a mechanistic changeover observed for **1-H$_2$O** and **1-OH** in their reactions with NO. The mechanistic interpretation offered is further substantiated by the results of water-exchange studies performed on the polyanionic porphyrin complex as a function of pH, temperature, and pressure.

Introduction

Iron porphyrins, an important class of transition-metal complexes, continue to attract considerable attention because of their importance in biology and catalysis. Roles played by these complexes in electron-transfer processes, metabolic control, transport and activation of oxygen under biological conditions, and versatile catalytic processes in vitro are surprisingly diverse. This rich chemistry stems partially from the fact that the reactivity of iron porphyrins is finely tuned by the surroundings of the central iron atom, such as the identity of axial ligands, the nature of the substituents on the tetrapyrrole ring, the polarity of the reaction medium (solvent or amino acid residues around the active site in heme proteins), and several other factors. To understand these structure−function relationships, numerous mechanistic and structural studies on heme proteins and their biomimetic models have been performed. In particular, synthetic iron(III) porphyrins, the structural analogues of prosthetic groups in ferriheme proteins, have been extensively studied in relation to their catalytic and biomimetic properties.

An important aspect of studies on the reactivity of model iron(III) porphyrins and ferriheme proteins concerns their interaction with nitric oxide.[1−10] These studies were directed, on the one hand, to explain the nature of interactions

* To whom correspondence should be addressed. E-mail: vaneldik@chemie.uni-erlangen.de.
[†] Institute for Inorganic Chemistry, University of Erlangen−Nürnberg.
[§] Institute for Organic Chemistry, University of Erlangen−Nürnberg.
[‡] Jagiellonian University.

(1) (a) Ford, P. C.; Lorkovic, I. M. *Chem. Rev.* **2002**, *102*, 993 and references cited therein. (b) Ford, P. C.; Laverman, L. E.; Lorkovic, I. M. *Adv. Inorg. Chem.* **2003**, *54*, 2003 and references cited therein.

10.1021/ic050924t CCC: $30.25
Published on Web 10/04/2005

underlying the diverse functions of NO in vivo and, on the other hand, to probe the reactivity of various iron porphyrins in ligand substitution reactions. In the latter context, studies on the mechanism of formation and decay of iron porphyrin nitrosyls provided information on the influence of the porphyrin ligand (modified in size and overall charge by the substituents on the tetrapyrrole ring)[1,2,4−7] and protein environment (in studies concerning heme proteins)[1,2,5,8−10] on the reactivity of the central Fe^{III} ion in ligand substitution reactions. Because the nature and lability of axial ligands coordinated to the iron center are of crucial importance for its overall reactivity, information gained from such mechanistic studies contributed to the understanding of various mechanistic pathways exhibited by iron porphyrins in their biological and catalytic functions.

It is now firmly established that binding of NO to an iron(III) porphyrin leads to the formation of a low-spin diamagnetic ($S = 0$) mononitrosyl complex, in which the Fe−N−O unit adopts a linear (or close to linear) geometry.[1,3] Because NO binding is accompanied by charge transfer from the NO ligand to the metal center, the resulting product (representing a $\{Fe-NO\}^6$ nitrosyl[3]) can be formally described as $(P)Fe^{II}$-NO^+. Detailed mechanistic investigations performed in our[5,6,9] and other[1,2,4,8,10] laboratories provided evidence that the dynamics of NO binding in heme proteins and synthetic iron porphyrins is to a large extent controlled by the ligand substitution step. Considerable differences in the rates of binding and release of NO,[1,2,4,6,8−10] and varying tendencies of the resulting nitrosyls to undergo subsequent reactions (such as reductive nitrosylation)[8,11,12] reported in these studies, apparently reflect the influence of variation in the immediate surroundings of the iron(III) center (mainly the types of axial ligands and porphyrin ring substituents) on the observed reactivity patterns. Despite these studies, a coherent pattern of a structure−reactivity relationship in the studied reactions is far from complete. In this context, systematic studies on the reactivity of water-soluble iron porphyrins (considered as model compounds for aqueous porphyrin chemistry) with different types of positively and negatively charged meso substituents toward NO have been initiated in order to better assess the correlation between the porphyrin structure and its reactivity.[4,6,7,11−14] The results of high-pressure NMR, stopped-flow, and laser flash photolysis investigations performed on these complexes provided evidence that the negatively charged peripheral substituents tend to labilize the axial metal−ligand bond by increasing the electron density on the metal center. A survey of literature data, however, shows that porphinatoiron(III) complexes may exist as five- or six-coordinate species in which the d electrons of the central Fe^{III} ion can be arranged into three possible spin states, viz., the low spin state ($S = {}^1/_2$), intermediate spin state ($S = {}^3/_2$) and the high spin state ($S = {}^5/_2$).[15] In addition, a range of $(P)Fe^{III}(L)_n$ complexes (with $n = 1$ or 2) with quantum mechanically admixed intermediate spin states ($S = {}^5/_2$ and ${}^3/_2$) have been reported, in which varying ratios of $S = {}^5/_2$ and ${}^3/_2$ admixing were observed, depending on the nature of the axial ligands and porphyrin ring substituents.[15−23] This variety of spin and ligation states is reflected in distinct structural features observed for different types of model and naturally occurring iron(III) porphyrins. While the low-spin $(P)Fe^{III}(L)_n$ complexes are typically six-coordinate and exhibit short axial and equatorial bonds (due to depopulation of e_g* orbitals), purely high-spin analogues are often five-coordinate, with elongated $Fe-N_p$ bonds and considerable displacement (0.4−0.6 Å) of the iron(III) center out of the porphyrin plane.[15,22] The structural manifestations of the intermediate spin state (admixed or pure) include short $Fe-N_p$ equatorial bonds (resulting from partial or complete depopulation of the $d_{x^2-y^2}$ orbital) and strongly elongated axial bonds.[15,17,21,23−25] Although these various features are critical in controlling the reactivity of the iron(III) porphyrins, their influence on the kinetic and mechanistic features of NO binding and release in different classes of $(P)Fe^{III}(L)_n$ complexes remains obscure. Taking into account a variety of spin and ligation states in heme proteins that can interact with NO under biological conditions, an improved characterization of typical reactivity

(2) Hoshino, M.; Laverman, L.; Ford, P. C. *Coord. Chem. Rev.* **1999**, *187*, 75 and references cited therein.
(3) (a) Wyllie, G. R. A.; Scheidt, W. R. *Chem. Rev.* **2002**, *102*, 1067 and references cited therein. (b) Ellison, M. K.; Schulz, Ch. E.; Scheidt, R. W. *J. Am. Chem. Soc.* **2002**, *124*, 13833 and references cited therein.
(4) Laverman, L. E.; Ford, P. C. *J. Am. Chem. Soc.* **2001**, *123*, 11614 and references cited therein.
(5) Wolak, M.; van Eldik, R. *Coord. Chem. Rev.* **2003**, *230*, 263 and references cited therein.
(6) Theodoridis, A.; van Eldik, R. *J. Mol. Catal. A: Chem.* **2004**, *224*, 197.
(7) (a) Imai, H.; Yamashita, Y.; Nakagawa, S.; Munakata, H.; Uemori, Y. *Inorg. Chim. Acta* **2004**, *357*, 2503. (b) Nakagawa, S.; Yashiro, T.; Munakata, H.; Imai, H.; Uemori, Y. *Inorg. Chim. Acta* **2003**, *349*, 17.
(8) Hoshino, M.; Maeda, M.; Konishi, R.; Seki, H.; Ford, P. C. *J. Am. Chem. Soc.* **1996**, *118*, 5702.
(9) (a) Franke, A.; Stochel, G.; Jung, Ch.; van Eldik, R. *J. Am. Chem. Soc.* **2004**, *126*, 4181. (b) Laverman, L. E.; Wanat, A.; Oszajca, J.; Stochel, G.; Ford, P. C.; van Eldik, R. *J. Am. Chem. Soc.* **2001**, *123*, 285.
(10) Hoshino, M.; Ozawa, K.; Seki, H.; Ford, P. C. *J. Am. Chem. Soc.* **1993**, *115*, 9568.
(11) Trofimova, N. S.; Safronov, A. Y.; Ikeda, O. *Inorg. Chem.* **2003**, *42*, 1945.
(12) Fernandez, B. O.; Lorkovic, I. M.; Ford, P. C. *Inorg. Chem.* **2004**, *43*, 5393.
(13) Laverman, L. E.; Hoshino, M.; Ford, P. C. *J. Am. Chem. Soc.* **1997**, *119*, 12663.
(14) Schneppensiepper, T.; Zahl, A.; van Eldik, R. *Angew. Chem., Int. Ed.* **2001**, *40*, 1678.
(15) Scheidt, W. R.; Reed, Ch. A. *Chem. Rev.* **1981**, *81*, 543.
(16) Toney, G. E.; Gold, A.; Savrin, J.; Haar, L. W.; Sangaiah, R.; Hatfield, W. E. *Inorg. Chem.* **1984**, *23*, 4350.
(17) Nesset, M. J. M.; Cai, S.; Shokhireva, T. K.; Shokhirev, N. V.; Jacobson, S. E.; Jayaraj, K.; Gold, A.; Walker, F. A. *Inorg. Chem.* **2000**, *39*, 532 and references cited therein.
(18) Evans, D. R.; Reed, Ch. *J. Am. Chem. Soc.* **2000**, *122*, 4660 and references cited therein.
(19) Ikezaki, A.; Nakamura, M. *Inorg. Chem.* **2002**, *41*, 6225 and references cited therein.
(20) Boersma, A. D.; Goff, H. M. *Inorg. Chem.* **1982**, *21*, 581.
(21) Simonato, J.-P.; Pecaut, J.; Pape, L. L.; Oddou, J.-L.; Jeandey, C.; Shang, M.; Scheidt, W. R.; Wojaczynski, J.; Wolowiec, S.; Latos-Grazynski, L.; Marchon, J.-C. *Inorg. Chem.* **2000**, *39*, 3978.
(22) Mazzanti, M.; Marchon, J.-C.; Wojaczynski, J.; Wolowiec, S.; Latos-Grazynski, L.; Shang, M.; Scheidt, W. R. *Inorg. Chem.* **1998**, *37*, 2476.
(23) Scheidt, W. R.; Osvath, S. R.; Lee, Y. J.; Reed, Ch. A.; Shaevitz, B.; Gupta, G. P. *Inorg. Chem.* **1989**, *28*, 1591.
(24) Yatsunyk, L. A.; Walker, F. A. *Inorg. Chem.* **2004**, *43*, 757.
(25) Gismelseed, A.; Bominaar, E. L.; Bill, E.; Trautwein, A. X.; Winkler, H.; Nasri, H.; Doppelt, P.; Mandon, D.; Fischer, J.; Weiss, R. *Inorg. Chem.* **1990**, *29*, 2741.

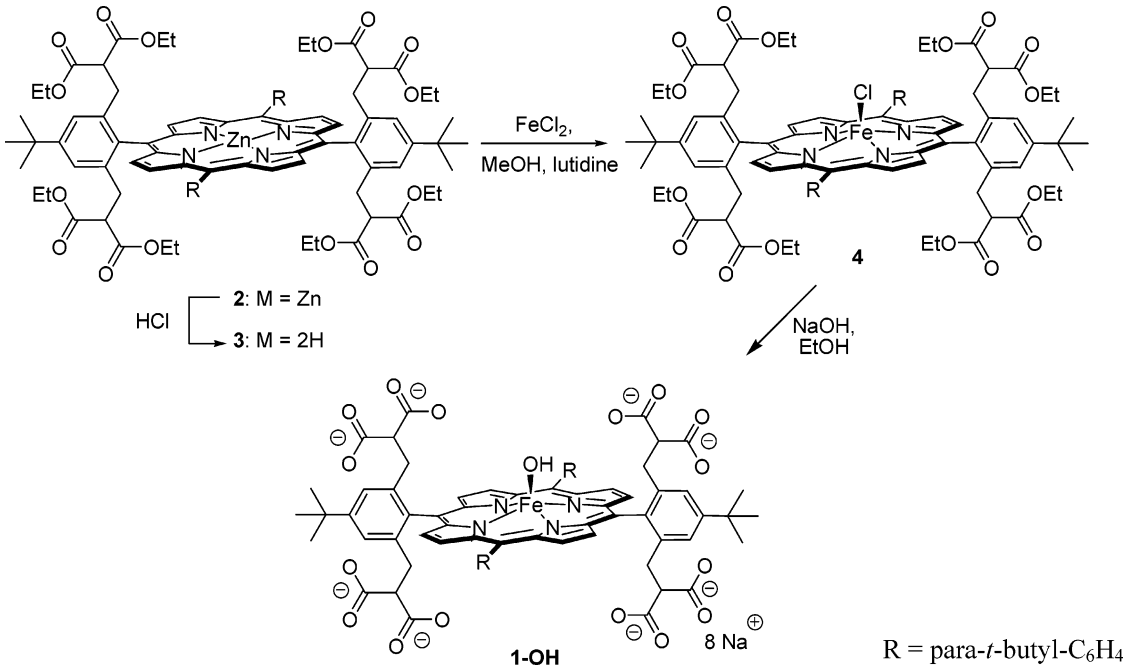

Figure 1. Synthesis of $(P^{8-})Fe^{III}$.

patterns observed in the reactions of NO with model five- and six-coordinate iron(III) porphyrins with high-spin, low-spin, and admixed intermediate-spin states of the central iron atom, respectively, would help to establish the relationship between the structure of the heme prosthetic group and its reactivity toward NO in various heme proteins.

In a continuation of our earlier mechanistic work on the reactivity of iron porphyrins toward NO,[5,6,9,14,26,27] we now report on the synthesis and spectroscopic characterization of a highly negatively charged water-soluble iron(III) porphyrin, $(P^{8-})Fe^{III}$ (**1**; compare Figure 1) and present the results of detailed mechanistic studies on its interaction with nitric oxide. Within this context, in addition to kinetic studies on the binding and release of NO from the diaqua $(P^{8-})Fe^{III}(H_2O)_2$ species present in aqueous solution at pH <9, the reactivity of a high-spin monohydroxo form of the complex formed at higher pH is reported. Temperature and pressure effects on the rates of NO binding and release obtained from stopped-flow and laser flash photolysis experiments at ambient and elevated pressure at low and high pH enabled the determination of activation parameters ($\Delta H^{\ddagger}$, $\Delta S^{\ddagger}$, and $\Delta V^{\ddagger}$) for the studied reactions. Activation volumes determined in these studies enabled the construction of volume profiles for the binding of NO to the diaqua and monohydroxo forms of the complex, respectively. On the basis of these data, a feasible explanation for the significant kinetic and mechanistic differences observed in the reactivity of these two species is offered. The results are compared with those reported for other water-soluble porphyrins and discussed in reference to the relevant literature data on the structure and reactivity of iron(III) porphyrins toward NO.

(26) Franke, A.; Stochel, G.; Suzuki, N.; Higuchi, T.; Okuzono, K.; van Eldik, R. *J. Am. Chem. Soc.* **2005**, *127*, 5360.
(27) Wolak, M.; van Eldik, R. *J. Am. Chem. Soc.* **2005**, in press.

Experimental Section

Synthesis and Characterization of 1. Chemicals and solvents employed for the synthesis of **1** were used as received unless otherwise noted. Solvents were dried using standard procedures. Column chromatography was performed on silica gel 60, 32−63 μm, 60 Å (MP Biomedicals). Standard ^{1}H and ^{13}C NMR spectra were recorded on a Bruker Avance 300 spectrometer (Bruker Analytische Messtechnik GmbH). Fast atom bombardment (FAB) mass spectrometry was performed with Micromass Zabspec and Varian MAT 311A machines. Electrospray ionization mass spectra (ESIMS) were measured in the negative ion mode on an ESI−FT−ICR−MS mass spectrometer (Fa. Agilent, ICR: APEX II, Fa. Bruker Daltonics, 7 T magnet). Standard UV−vis spectra were recorded on a Shimadzu UV-3102 PC UV−vis−NIR scanning spectrophotometer. IR spectra (KBr pellets) were recorded with a FT-IR IFS 88 infrared spectrometer (Bruker Analytische Messtechnik GmbH). Elemental analyses were carried out on a CHN-Mikroautomat (Heraeus). Thin-layer chromatography was carried out on E. Merck silica gel 60 F254 plates. Zinc(II) 5^4,10^4,15^4,20^4-tetra-*tert*-butyl-5^2,5^6,15^2,15^6-tetrakis[2,2-bis(ethoxycarbonyl)ethyl]-5,10,15,20-tetraphenylporphyrin (**2**) was synthesized as described previously.[28]

5^4,10^4,15^4,20^4-Tetra-*tert*-butyl-5^2,5^6,15^2,15^6-tetrakis[2,2-bis(ethoxycarbonyl)ethyl]-5,10,15,20-tetraphenylporphyrin (3). HCl (6 M, 50 mL) was added to a solution of **2** (174 mg, 0.109 mmol) in CH_2Cl_2 (50 mL), and the two layers were shaken vigorously. The green (organic) layer was shaken once again with 2 M HCl (50 mL) and twice with water (50 mL each). After neutralization with a saturated $NaHCO_3$ solution (50 mL) and a final washing with brine (50 mL), the organic layer was dried with $MgSO_4$ and the solvent was removed under reduced pressure. The compound was further cleaned by column chromatography (silica gel, CH_2Cl_2/ethyl acetate 19:1) and obtained as a purple powder. Yield: 160 mg (96%, 0.105 mmol). ^{1}H NMR (300 MHz, $CDCl_3$, rt): δ 8.88

(28) Guldi, D. M.; Zilbermann, I.; Anderson, G.; Li, A.; Balbinot, D.; Jux, N.; Hatzimarinaki, M.; Prato, M. *Chem. Commun.* **2004**, 726.

(d, 4H, ^3J = 4.78 Hz, β-pyrr−H), 8.69 (d, 4H, ^3J = 4.8 Hz, β-pyrr−H), 8.15 (d, 4H, ^3J = 8.1 Hz, *o*-Ar*−H; an asterisk indicates proton resonances of the charge-carrying aryl ring), 7.76 (d, 4H, ^3J = 8.1 Hz, *m*-Ar*−H), 7.46 (s, 4H, *m*-Ar−H), 3.62 (m, 16H, OCH_2CH$_3$), 3.04 (t, 4H, ^3J = 7.8 Hz, CH), 2.80 (d, 8H, ^3J = 7.8 Hz, Ar−CH_2), 1.60 (s, 36H, CH_3), 1.51 (s, 36H, CH_3), 0.69 (t, 24H, ^3J = 7.2 Hz, OCH$_2$CH_3). ^{13}C NMR (75 MHz, $CDCl_3$, rt): δ 168.4, 151.4, 150.5, 139.3, 138.7, 138.4, 134.5, 132.0, 130.1, 124.4, 123.6, 120.2, 115.2, 60.7, 52.2, 34.8, 33.6, 31.6, 31.5, 29.6, 13.4. MS (FAB, NBA): *m*/*z* 1528 ($M^{+\cdot}$). IR (KBr): ν [cm^{-1}] 3318, 2961, 2933, 2906, 2867, 1755, 1735, 1632, 1468, 1367, 1221, 1146, 1034, 807. UV−vis (CH_2Cl_2): λ [nm] (ϵ [L mol^{-1} cm^{-1}]) 421 (4.58×10^5), 517 (1.98×10^4), 551 (8.1×10^3), 591 (6.4×10^3), 648 (4.3×10^3). Anal. Calcd for $C_{92}H_{110}N_4O_{16}$: C, 72.32; H, 7.26; N, 3.67. Found: C, 71.97; H, 7.31; N, 3.66.

Chloroiron(III) 5^4,10^4,15^4,20^4-Tetra-*tert*-butyl-5^2,5^6,15^2,15^6-tetrakis[2,2-bis(ethoxycarbonyl)ethyl]-5,10,15,20-tetraphenylporphyrin (4). A solution of $FeCl_2$ (400 mg, 3.15 mmol) in ethanol (30 mL) was added to a solution of **3** (343 mg, 0.225 mmol) in $CHCl_3$ and the mixture heated under reflux for 18 h. The solvent was evaporated and the residue dissolved in CH_2Cl_2 and washed with 6 M HCl. The organic layer was separated and washed twice with water. After drying over $MgSO_4$, the compound was cleaned by column chromatography (silica gel, 19:1 CH_2Cl_2/ethyl acetate) to give a dark green powder. Yield: 318 mg (89%, 0.201 mmol). ^{1}H NMR (300 MHz, $CDCl_3$, rt): δ 82.9 (br s, β-pyrr−H), 80.8 (br s, β-pyrr−H), 15.8, 14.1, 13.3, 12.2 (br s, aryl−H). MS (FAB, NBA): *m*/*z* 1582 (M^+). IR (KBr): ν [cm^{-1}] 2963, 2939, 2907, 2869, 1751, 1734, 1626, 1464, 1445, 1395, 1367, 1332, 1149, 1031, 997, 859, 803, 722. UV−vis (CH_2Cl_2): λ [nm] (ϵ [L mol^{-1} cm^{-1}]) 422 (1.18×10^5), 509 (1.4×10^4), 583 (7.3×10^3). Anal. Calcd for $C_{92}H_{108}ClFeN_4O_{16}\cdot CH_2Cl_2$: C, 65.62; H, 6.51; N, 3.29. Found: C, 65.58; H, 6.68; N, 3.33.

Octasodium Hydroxoiron(III) 5^4,10^4,15^4,20^4-Tetra-*tert*-butyl-5^2,5^6,15^2,15^6-tetrakis[2,2-bis(carboxylato)ethyl]-5,10,15,20-tetraphenylporphyrin (1-OH). NaOH (1.50 g, 37.5 mmol) was added to a solution of **4** (200 mg, 0.126 mmol) in ethanol (20 mL), and the reaction mixture was heated under reflux for 1 h. After cooling to room temperature, the precipitate was filtered, washed with ethanol (200 mL), and dried under reduced pressure. Gel permeation chromatography (Sephadex LH20) in methanol und subsequent precipitation with diethyl ether gave a dark brown powder, which, according to the microanalysis, contains sodium hydroxide in the lattice. Yield: 230 mg (83%, 0.105 mmol; based on the formula obtained by microanalysis). ^{1}H NMR (300 MHz, unbuffered D_2O, pD = 13.4, rt): δ 82.7 (br s, β-pyrr−H), 13.2, 12.3 (br s, aryl−H). ESIMS (MeOH/H_2O): 1376.45 {[(P)Fe^{III}(COOH)$_5$(COO)$_2$-(COONa)]$^-$}, 1354.46 {[(P)Fe^{III}(COOH)$_6$(COO)$_2$]$^-$}. IR (KBr): ν [cm^{-1}] 3429, 2963, 2924, 2854, 1594, 1445, 884, 805. UV−vis (H_2O, pH 11): λ [nm] (ϵ [L mol^{-1} cm^{-1}]) 417 (1.1×10^5), 532 (1.2×10^4). Anal. Calcd for $C_{76}H_{69}FeN_4Na_8O_{17}\cdot 16NaOH$: C, 41.68; H, 3.91; N, 2.56. Found: C, 41.81; H, 4.04; N, 1.56.

Materials. NO gas (Messer Griesheim or Riessner Gase, ≥99.5 vol %) was cleaned from trace amounts of higher nitrogen oxides by passing it through a concentrated KOH solution and an Ascarite II column (NaOH on silica gel, Sigma-Aldrich). CAPS, MES, Tris, and Bis-Tris buffers were purchased from Sigma-Aldrich. All other chemicals used in this study were of analytical reagent grade.

Solution Preparation. All solutions were prepared from deionized water. Buffered solutions of the appropriate pH for laser flash photolysis and stopped-flow measurements were prepared with the use of Tris (0.05 M), Bis-Tris (0.05 M), CAPS (0.05 M), and TAPS (0.05 M) buffers. The desired pH was adjusted by the addition of $HClO_4$ or NaOH. The ionic strength (0.1 M) was adjusted with $NaClO_4$. Argon or nitrogen and gastight glassware were used for the preparation and handling of deoxygenated solutions.

Measurements. pH measurements were performed on a Methrom 623 pH meter. An NO electrode (World Precision Instruments isolated nitric oxide meter, model ISO-NO) was used to determine the concentration of NO gas in aqueous solution. The NO electrode was calibrated with a freshly prepared KNO_2 solution according to the method suggested by the manufacturer. UV−vis spectra were recorded in gastight cuvettes on a Shimadzu UV-2100 spectrophotometer equipped with a thermostated (±0.1 °C) cell compartment.

Kinetic Studies. (a) Laser Flash Photolysis. Laser flash photolysis was carried out with the use of the LKS-60 spectrometer from Applied Photophysics for detection and a Nd:YAG laser (SURLITE I-10, Continuum) pump source operating in the third harmonic (λ_{exc} = 355 nm) (100-mJ pulses with ∼7-ns pulse widths). Spectral changes at 427 and 432 nm (at pH 7 and 11, respectively) were monitored using a 100-W xenon lamp, monochromator, and photomultiplier PMT-IP22. The absorbance reading was balanced to zero before the flash. Data were recorded on a digital storage oscilloscope DSO HP 54522A and transferred to a computer unit for subsequent analysis. Gastight quartz flow cuvettes and a pill-box cell combined with a high-pressure unit were used at ambient and elevated pressures (up to 170 MPa), respectively. In ambient-pressure experiments, the deoxygenated solution of the iron porphyrin was mixed in an appropriate volume ratio with the NO-saturated solution, transferred to a gastight flow cuvette, and equilibrated in a thermostated cell holder for 10 min. In the high-pressure studies, deoxygenated solutions of iron porphyrin and NO were mixed in an appropriate ratio with the use of gastight syringes, transferred under an inert atmosphere to the pill-box cell, and equilibrated for 10 min at the appropriate temperature and pressure in the high-pressure cell compartment.

All kinetic experiments were performed under pseudo-first-order conditions, i.e., with at least 10-fold excess of NO over the iron porphyrin. Rate constants reported are the mean values of at least five kinetics runs, and the quoted uncertainties are based on the standard deviation.

(b) Stopped-Flow Measurements. Stopped-flow kinetic measurements were performed on an SX 18.MV (Applied Photophysics) stopped-flow apparatus. In a typical experiment, a deoxygenated buffer solution was mixed in varying volume ratios with a NO-saturated solution in a gastight syringe to obtain the appropriate NO concentration (0.2−1.8 mM). The NO solution was then rapidly mixed with deoxygenated iron(III) porphyrin in a 1:1 volume ratio in a stopped-flow apparatus. The kinetics of the reaction was monitored at 427 and 432 nm at pH 7 and 11, respectively. The rates of NO binding and release (k_{on} and k_{off}) were determined from slopes and intercepts of linear plots of k_{obs} versus [NO], respectively, as described in more detail in the Results and Discussion section. The NO dissociation rates at different temperatures and pressures were also measured directly by the NO-trapping method. This involved rapid mixing of a (P^{8-})Fe^{II}(NO$^+$)(L) solution (2×10^{-5} M; L = H_2O and OH^- at pH 7 and 11, respectively) containing a small excess of NO with aqueous solutions of [Ru^{III}(edta)(H_2O)]$^-$ (1−2 mM) to give [Ru^{III}(edta)NO]$^-$ and (P^{8-})Fe^{III}(L), as evidenced by the observed spectral change. The kinetics of NO release was followed in a stopped-flow spectrophotometer at 427 nm (pH 7) or 432 nm (pH 11). The first-order rate constants determined from the kinetic traces were in acceptable agreement with those determined from the intercepts of the plots of k_{obs} versus [NO].

High-pressure stopped-flow experiments were performed at pressures up to 130 MPa on a custom-built instrument described

previously.[29] The kinetic traces were analyzed with the use of the OLIS KINFIT (Bogart, GA, 1989) set of programs.

(c) ^{17}O NMR Water-Exchange Measurements. Rate and activation parameters for water exchange on the paramagnetic $(P^{8-})Fe^{III}(H_2O)_2$ complex and the corresponding activation parameters $\Delta H^{\ddagger}_{ex}$, $\Delta S^{\ddagger}_{ex}$, and $\Delta V^{\ddagger}_{ex}$ were measured by use of the ^{17}O NMR line-broadening technique. Aqueous solutions of **1** (20 mM) were prepared at pH 7 (0.05 M Bis-Tris buffer) and 11 (0.05 M CAPS buffer), and 10% of the total sample volume of enriched ^{17}O-labeled water (normalized 19.2% ^{17}O H_2O, D-Chem Ltd.) was added to the solution.

A sample containing the same components except for **1** was used as the reference. Variable-temperature and -pressure Fourier transform ^{17}O NMR spectra were recorded at a frequency of 54.24 MHz on a Bruker Advance DRX 400WB spectrometer. The temperature dependence of the ^{17}O line broadening was determined in the range of 278−353 K. A homemade high-pressure probe[30] was used for the variable-pressure experiments performed at pH 7 at the selected temperature (283 K) and in the pressure range of 1−150 MPa. The sample was placed in a standard 5-mm NMR tube cut to a length of 45 mm. The pressure was transmitted to the sample by a movable macor piston, and the temperature was controlled as described elsewhere.[30] The reduced transverse relaxation times ($1/T_{2r}$) were calculated for each temperature and pressure from the difference in the line widths observed in the presence and absence of the metal complex ($\Delta\nu_{obs} - \Delta\nu_{solvent}$). The reduced transverse relaxation time is related to the exchange rate constant $k_{ex} = 1/\tau_m$ (where τ_m is the mean-coordinated solvent lifetime) and to the NMR parameters by the Swift and Connick equation (1),[31a,b]

$$\frac{1}{T_{2r}} = \pi\frac{1}{P_m}(\Delta\nu_{obs} - \Delta\nu_{solvent}) = \frac{1}{\tau_m}\left\{\frac{T_{2m}^{-2} + (T_{2m}\tau_m)^{-1} + \Delta\omega_m^{2}}{(T_{2m}^{-1} + \tau_m^{-1})^2 + \Delta\omega_m^{2}}\right\} + \frac{1}{T_{2os}} \quad (1)$$

where P_m is the mole fraction of water coordinated to the Fe^{III} ion, T_{2os} represents the outer-sphere contribution to T_{2r} arising from long-range interactions of unpaired electrons of Fe^{III} with the water outside the coordination sphere, T_{2m} is the transverse relaxation time of water in the inner coordination sphere in the absence of chemical exchange, and $\Delta\omega_m$ is the difference in the resonance frequency of ^{17}O nuclei in the first coordination sphere of the metal and in the bulk solvent. In the present system, the contributions of $1/T_{2m}$ and $1/T_{2os}$ to $1/T_{2r}$ are negligible, so that eq 1 can be reduced to eq 2. Taking into account that the temperature dependence of

$$\frac{1}{T_{2r}} = \pi\frac{1}{P_m}(\Delta\nu_{obs} - \Delta\nu_{solvent}) = \frac{1}{\tau_m}\left\{\frac{\Delta\omega_m^{2}}{\tau_m^{-2} + \Delta\omega_m^{2}}\right\} \quad (2)$$

k_{ex} is given by eq 3 (taken from transition-state theory), the NMR

$$k_{ex} = 1/\tau_m = (k_B T/h)\exp\{(\Delta S^{\ddagger}_{ex}/R) - (\Delta H^{\ddagger}_{ex}/RT)\} \quad (3)$$

and kinetic parameters were calculated by the use of a nonlinear least-squares method applied to eq 2, in which $1/\tau_m$ was replaced by eq 3. The temperature dependence of $\Delta\omega_m$ was assumed to be a simple reciprocal function A/T,[31a−c] where A was determined as a parameter in the treatment of the line-broadening data. The exchange rate constant is assumed to have a simple pressure dependence given by eq 4, where k_{ex}^{0} is the rate constant for solvent

$$k_{ex} = 1/\tau_m = k_{ex}^{0}\exp\{(-\Delta V^{\ddagger}_{ex}/RT)P\} \quad (4)$$

exchange at atmospheric pressure. The pressure-dependent measurements were performed at a temperature close to the optimal exchange region [i.e., around the maximum of the plot of $\ln(1/T_{2r})$ versus $1/T$]. The reduced relaxation time T_{2r} and the value of $\Delta\omega_m$ (calculated using the value of A determined from the temperature dependence and assumed to be pressure-independent[31d]) were substituted into eq 2 to determine k_{ex} at each pressure. The resulting plot of $\ln(k_{ex})$ versus pressure was linear, and the volume of activation was calculated directly from the slope ($-\Delta V_{ex}^{\ddagger}/RT$). The value of k_{ex}^{0} obtained from the plot of $\ln(k_{ex})$ versus P by extrapolation to atmospheric pressure was in good agreement with the corresponding value of k_{ex}^{0} from the temperature-dependent measurements at ambient pressure.

In analogous temperature-dependent ^{17}O NMR measurements performed for the studied iron(III) porphyrin at pH 11 (0.05 M CAPS buffer), the line widths observed in the presence and absence of the metal complex changed little (6−13 Hz within the temperature range of 278−353 K), indicating the absence of a significant water-exchange process for the **1** form present at higher pH. Because of the small observed effects (close to the experimental error limits), the data obtained in the variable-temperature study did not allow a reliable fit to the Swift and Connick equation.

Results and Discussion

Synthesis of 1. Some of us recently reported the synthesis of a water-soluble anionic zinc porphyrin (**2** in Figure 1) that carries eight carboxylates in four malonate units.[28] The precursor porphyrin **2** carries the malonates in the form of ethyl esters, which renders the compound soluble in organic but not in aqueous solvents. We choose **2** as a starting material because it can be easily made from a bromomethylated zinc porphyrin precursor[32] by a typical malonate ester alkylation protocol. By virtue of its easy demetalation with concentrated hydrochloric acid, **2** is transformed into the free-base porphyrin **3**, as shown in Figure 1. Subsequent reaction with ferrous chloride in methanol using lutidine as a proton scavenger gives the neutral iron(III) porphyrin tetramalonic ester system, **4**. ^{1}H NMR and UV−vis spectroscopic data show that **4** is a paramagnetic iron(III) porphyrin with a single chloro axial ligand. The two β-pyrrole ^{1}H resonances at 82.9 and 80.8 ppm (half-width ∼ 300 Hz) indicate the overall C_{2v} symmetry of the porphyrin and prove the $S = {}^5/_2$ spin state.[33,34] Saponification of the malonic esters of **4** with sodium hydroxide in ethanol leads to precipitation of a brownish material that is soluble in water but totally insoluble in apolar solvents. Gel permeation chromatography (Sephadex LH20) in methanol and subsequent precipitation with diethyl ether gave a solid material containing 75% of **1** (with the impurities being NaOH and H_2O). Standard NMR spectra

(29) (a) van Eldik, R.; Palmer, D. A.; Schmidt, R.; Kelm, H. *Inorg. Chim. Acta* **1981**, *50*, 131. (b) van Eldik, R.; Gaede, W.; Wieland, S.; Kraft, J.; Spitzer, M.; Palmer, D. A. *Rev. Sci. Instrum.* **1993**, *64*, 1355.
(30) Zahl, A.; Neubrand, A.; Aygen, S.; van Eldik, R. *Rev. Sci. Instrum.* **1994**, *65*, 882.
(31) (a) Swift, T. J.; Connick, R. E. *J. Chem. Phys.* **1962**, *37*, 307. (b) Swift, T. J.; Connick, R. E. *J. Chem. Phys.* **1964**, *41*, 2553. (c) Bloembergen, N. J. *J. Chem. Phys.* **1957**, *27*, 595. (d) Newman, K. E.; Meyer, F. K.; Merbach, A. E. *J. Am. Chem. Soc.* **1979**, *101*, 1470.
(32) Jux, N. *Org. Lett.* **2000**, *2*, 2129.
(33) Woon, T. C.; Shirazi, A.; Bruice, T. *Inorg. Chem.* **1986**, *25*, 3845.
(34) Cheng, R.-J.; Latos-Grazynski, L.; Balch, A. *Inorg. Chem.* **1982**, *21*, 2412.

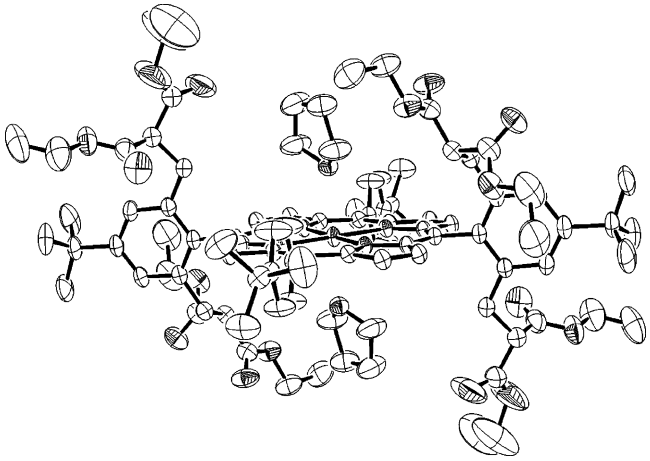

Figure 2. ORTEP diagram of [(P)Zn(THF)$_2$] (**2-THF**) visualizing structural features of the porphyrin ligand in **2**. General crystallographic data for **2-THF** are reported in Table S1 of the Supporting Information.

measured in unbuffered D_2O ([**1**] = 1.5×10^{-2} M, pD = 13.4) have shown that under these conditions **1** exists as a high-spin monohydroxo complex (P^{8-})$Fe^{III}OH$ (β-pyrrole ^1H at 82.7 ppm; see also further text).

To visualize the structure of the porphyrin ligand in **1**, the crystal structure of its zinc precursor **2** crystallized from THF is shown in Figure 2. As can be seen from the structure, the zinc atom lies in the N_4 porphyrin plane (average Zn−N distance, 2.053 Å) and interacts weakly with oxygen atoms of the two axially bound THF molecules (Zn−O distance, 2.419 Å). Two structural features important in terms of the investigations presented in this report can be extracted from this structure. First, the malonate groups are located above and below the porphyrin plane, thus decreasing the possibility of μ-oxo-dimer formation for steric and electrostatic reasons (as confirmed by in-depth spectroscopic studies described below). Second, the malonate groups cannot coordinate to the metal center in an intramolecular fashion without extreme distortion of the molecule (the average distance of the malonate oxygen atoms from the zinc atom, ∼7 Å; the closest distance, ∼4 Å). Nevertheless, ester or carboxylate groups of malonate substituents may interact with axial ligands coordinated to the metal center, as visualized in Figure S1 (in the Supporting Information) for the diaqua-ligated porphyrin (P^{8-})$Fe^{III}(H_2O)_2$.

Speciation of 1 as a Function of pH. To establish the nature of the iron porphyrin species present in aqueous solution as a function of pH, a spectrophotometric titration in the pH 1−12 range and ^1H NMR measurements at selected pD values (7 and 11) were performed for **1**. Figure 3 shows the UV−vis spectral changes observed during the spectrophotometric titration of **1** at 0.1 M ionic strength (adjusted with $NaClO_4$). The corresponding plot of absorbance at 418 nm versus pH is shown in the inset of Figure 3b. As can be seen from these data, the observed spectral changes can be separated into two regions. In the pH 1−6 range, a continuous increase in absorbance over the whole spectral range is observed. This results mainly from an increase in the solubility of the porphyrin complex due to deprotonation of the carboxylic acid groups upon increasing pH. A concomitant gradual shift of the broad band centered at ca. 420 nm to shorter wavelengths leads to the formation of a Soret band at 400 nm ($\epsilon = 9.8 \times 10^4$ M^{-1} cm^{-1}) at pH >5. Further spectral changes, accompanied by clean isosbestic points at 360, 438, 514, and 555 nm, are observed in the pH 8−11 range. The nature of these spectral changes, i.e., shift of the Soret band to 417 nm ($\epsilon = 1.1 \times 10^5$ M^{-1} cm^{-1}) and formation of peaks at 334 and 532 nm ($\epsilon = 1.2 \times 10^4$ M^{-1} cm^{-1}), is analogous to that observed for other water-soluble iron(III) porphyrins on deprotonation of coordinated water at the Fe(III) center.[35−39] The spectral features observed at high pH are typical for that reported for monomeric monohydroxo-coordinated iron(III) porphyrins in organic[33,34] and aqueous[35−39] solvents. No further spectral changes occurred in solution at high pH on extended standing, and those observed in the pH 8−11 range were fully reversible and indicated rapid interconversion of species present at high and low pH upon changing of the pH. These observations strongly suggest that the formation and hydrolysis of μ-oxo dimers do not occur in the studied system, as was further confirmed by NMR data reported below.

The pK_{a1} values characterizing the acid−base equilibria in the studied system were determined by Specfit[40] analysis of the UV−vis spectra recorded in the pH 1−12 range. To minimize experimental errors resulting from changes in absorbance due to the observed precipitation of protonated (H_8P)Fe^{III} in the pH 1−5 range, the results of four independent titrations were subjected to the Specfit analysis. The pK_a values of 2.9 ± 0.8 and 4.4 ± 0.6 estimated for the low pH range[41a] are ascribed to deprotonation of the carboxylic acid groups on the porphyrin (compare simplified eq 5) on the basis of their similarity with the pK_{a1} of carboxylic groups in benzylmalonic acid (2.56 and 5.22),[41b] and the observed changes in the solubility of **1** in this pH range. The pK_{a1}

$$(H_8P)Fe^{III} \rightleftarrows (P^{8-})Fe^{III} + 8H^+ \qquad 2.5 < pK_{a(RCOOH)} < 5.2 \tag{5}$$

value of 9.26 ± 0.01 determined at higher pH is ascribed to deprotonation of a water molecule in the (P^{8-})$Fe(H_2O)_2$ (**1-H_2O)** species present in solution at pH <9, according to eq 6. This conclusion is further supported by ^1H NMR data and

$$(P^{8-})Fe^{III}(H_2O)_2 \rightleftarrows (P^{8-})Fe^{III}(OH) + H_3O^+ \qquad pK_{a1} \tag{6}$$

^{17}O NMR water-exchange measurements performed for **1** at pD 7 and 11. According to numerous literature reports, ^1H

(35) Zipplies, M. F.; Lee, W. A.; Bruice, T. C. *J. Am. Chem. Soc.* **1986**, *108*, 4433.
(36) Tondreau, G. A.; Wilkins, R. G. *Inorg. Chem.* **1986**, *25*, 2745.
(37) Kobayashi, N. *Inorg. Chem.* **1985**, *24*, 3324.
(38) Miskelly, G. M.; Webley, W. S.; Clark, Ch. R.; Buckingham, D. A. *Inorg. Chem.* **1988**, *27*, 3773.
(39) El-Awady, A. A.; Wilkins, P. C.; Wilkins, R. G. *Inorg. Chem.* **1985**, *24*, 2053.
(40) Binstead, R. A.; Jung, B.; Zuberbühler, A. D. Specfit. 32, Spectrum Software Associates, 2000.
(41) (a) Mean pK_a values determined in four independent measurements. (b) Kawassiades, C. Th.; Kouimtzis, Th. A.; Tossidis, J. A. *Chem. Chron. A* **1968**, *33*, 1. *The Handbook of Chemistry and Physics* (76th ed.; CRC Press: New York, 1995) reports the values p$K_a(1) = 2.83$ and p$K_a(2) = 5.69$.

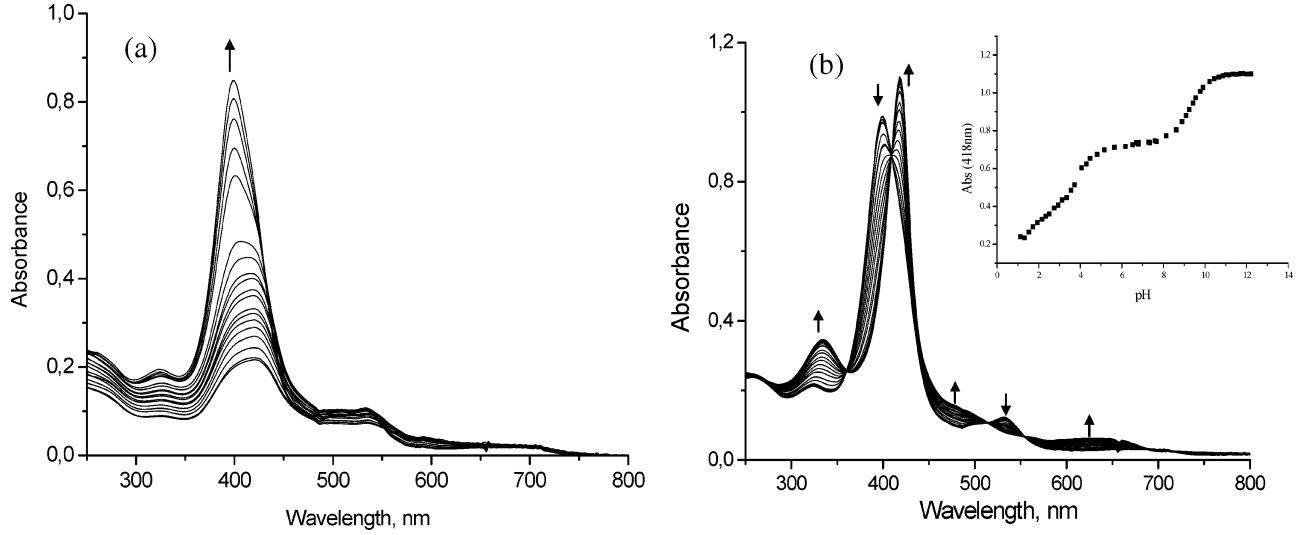

Figure 3. UV−vis spectral changes observed for aqueous solutions of $(P^{8-})Fe^{III}$ (**1**) in the pH 1−6 (a) and 6−12 (b) ranges. Inset: plot of absorbance at 418 nm versus pH. Experimental conditions: [**1**] = 1×10^{-5} M, 25 °C, I = 0.1 M (adjusted with $NaClO_4$).

NMR spectroscopy is a widely recognized method to characterize $(P)Fe(L)_n$ (n = 1 and 2) complexes in solution.[16−19,24,42−45] The hyperfine shift patterns observed for paramagnetic iron porphyrins were shown to strongly depend on the spin and ligation states of the central iron atom. In particular, the chemical shift of the β-pyrrole protons in iron(III) porphyrins has proven to be an excellent probe to determine the spin state of the iron(III) center.[16−19,24,42−45] In the case of pure high-spin ($S = {}^5/_2$) iron(III) porphyrins, the β-pyrrole proton signals are shifted downfield to $\delta \geq 80$ ppm at 25 °C.[18,19,33,34] In contrast, the pure intermediate spin state ($S = {}^3/_2$) complexes exhibit β-pyrrole proton signals at extremely upfield positions, i.e., at ca. −60 ppm.[18] In the case of admixed intermediate spin state complexes ($S = {}^5/_2$, ${}^3/_2$), β-pyrrole resonances appear between these two extremes, viz., +80 and −60 ppm. As can be seen from the data summarized in Table 1, the β-pyrrole shifts observed for selected water-soluble iron(III) porphyrins fall in the range of 43−85 ppm. Chemical shifts of $\delta \geq 80$ ppm, diagnostic for monomeric monohydroxo-ligated iron porphyrins in aqueous[35,42,43] and nonaqueous[18,33,34] solvents, clearly indicate that these complexes exist in solution as purely high-spin species. The more upfield signals (43−73 ppm) observed for diaqua-ligated forms[35,43,44] reflect a varying contribution of $S = {}^3/_2$ in the admixed $S = {}^3/_2$, ${}^5/_2$ spin system featuring $(P)Fe(H_2O)_2$, in which the axial sites are occupied by two weak field H_2O ligands (see also the text below). The position of the β-pyrrole proton resonances at ca. 47 ppm for $(P^{8-})Fe$ at pH 7 (compare Table 1 and Figure S2 in the Supporting Information) is similar to that observed for the diaqua forms of other negatively charged water-soluble iron(III) porphyrins and differs remarkably from that observed for the monohydroxo species. A peak at ca. 83 ppm (Table 1 and Figure S2b in the Supporting Information) appears, however, in the ^{1}H NMR spectrum of $(P^{8-})Fe$ at pD 11, indicating the presence of the monohydroxo-coordinated form. In addition, the lack of resonances in the spectral region of 13−14 ppm (characteristic for β-pyrrole protons in μ-oxo-bridged

Table 1. β-Pyrrole ^{1}H NMR Chemical Shifts[a] and pK_{a1} Values of Synthetic Water-Soluble Iron(III) Porphyrins

Iron(III) porphyrin	*meso* phenyl substituent	β-pyrrole ^{1}H (ppm)[a]		pK_{a1}[b]
		$(P)Fe(H_2O)_2$	$(P)Fe(OH)$	
$(P^{8-})Fe$[c]	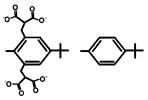	45.6; 46.7[d]	82.7	9.3[c]
$(TanP^{4-})Fe$[e]		NA	NA	8.0
$(TPPS^{4-})Fe$[f]		52.4	NA[g]	7.0
$(DMPS^{4-})Fe$[h]		45	80	7.0
$(TMPS^{4-})Fe$[i]		43	82	6.9
$(TF_4TMAP^{4+})Fe$[j]		72	85	6.0
$(4\text{-}TMPyP^{4+})Fe$[f]		70.5	NA	5.5
$(2\text{-}TMPyP^{4+})Fe$[k]		73.5	84	5.1

[a] Referenced to TMPS. NA = not assigned. [b] Values from ref 53 unless otherwise stated. [c] This work. [d] Two separate resonances result from chemical inequivalency of β-pyrrole protons in P^{8-}. [e] Reference 7a. [f] Reference 44. [g] The small peak at 33.4 ppm assigned to the hydroxo form of $(TPPS)Fe^{III}$ in ref 44 is probably shifted upfield from the typical value of ca. 80 ppm because of the exchange of diaqua, monohydroxo, and μ-oxo dimers present in solution at pD 5−6. [h] Reference 35. [i] Reference 27. [j] Reference 42. [k] Reference 43.

(42) (a) La, T.; Miskelly, G. M. *J. Am. Chem. Soc.* **1995**, *117*, 3613. (b) La, T.; Miskelly, G. M.; Bau, R. *Inorg. Chem.* **1997**, *36*, 5321.
(43) Reed, R. A.; Rodgers, K. R.; Kushmeider, K.; Spiro, T. *Inorg. Chem.* **1990**, *29*, 2883.
(44) Ivanca, M. A.; Lappin, A. G.; Scheidt, W. R. *Inorg. Chem.* **1991**, *30*, 711.
(45) Walker, F. A. Proton and NMR spectroscopy of paramagnetic metalloporphyrins. In *The Porphyrin Handbook*; Kadish, K. M., Smith, K. M., Guilard, R., Eds.; Academic Press: New York, 1999; Vol. 5.

Table 2. Rate Constants (at 25 °C) and Activation Parameters for Water-Exchange Reactions on a Series of Water-Soluble Iron(III) Porphyrins

iron(III) porphyrin	$\delta_{\beta-\text{pyrrole}}$ (ppm)	Int %[a]	k_{ex} (s^{-1})	$\Delta H^{\ddagger}_{ex}$ (kJ mol^{-1})	$\Delta S^{\ddagger}_{ex}$ (J mol^{-1} K^{-1})	$\Delta V^{\ddagger}_{ex}$ (cm^3 mol^{-1})
1-H_2O[b]	ca. 46	24	$(7.7 \pm 0.1) \times 10^6$	61 ± 6	$+91 \pm 23$	$+7.4 \pm 0.4$
$(TMPS^{4-})Fe(H_2O)_2$[c]	43	26	$(2.1 \pm 0.1) \times 10^7$	61 ± 1	$+100 \pm 5$	$+11.9 \pm 0.3$
$(TPPS^{4-})Fe(H_2O)_2$[c]	52	20	$(2.0 \pm 0.1) \times 10^6$	67 ± 2	$+99 \pm 10$	$+7.9 \pm 0.2$
$(TMPyP^{4+})Fe(H_2O)_2$[c]	70.5	6.8	$(4.5 \pm 0.1) \times 10^5$	71 ± 2	$+100 \pm 6$	$+7.4 \pm 0.4$

[a] Calculated according to eq 7. [b] This work. [c] Reference 14.

dimers[18,34,44]), shows unequivocally that the studied porphyrin complex does not undergo dimerization to a μ-oxo dimer at high pH.

Temperature- and pressure-dependent ^{17}O NMR studies performed at pH 7 (compare the Experimental Section and Figure S3a,b in the Supporting Information) indicated that the $(P^{8-})Fe(H_2O)_2$ form (**1-H_2O**) present at this pH undergoes a rapid water-exchange reaction. As can be seen from data presented in Table 2, the rate constant measured for this process ($k_{ex} = 7.7 \times 10^6$ s^{-1} at 25 °C) falls within the range of k_{ex} values reported for diaqua-ligated forms of other water-soluble iron(III) porphyrins. Significantly positive $\Delta S^{\ddagger}_{ex}$ and $\Delta V^{\ddagger}_{ex}$ observed for **1-H_2O** as well as for other diaqua-ligated porphyrins indicate the operation of a dissociative (I_d or D) pathway for water exchange on $(P)Fe^{III}(H_2O)_2$ complexes studied to date. In contrast to this observation, variable-temperature ^{17}O NMR measurements performed for **1** at pH 11 indicated very small variation of the reduced relaxation time for the bulk water signal (compare Figure S3c in the Supporting Information). This strongly suggests that the monohydroxo-ligated form of **1** exists in the five-coordinate form $(P^{8-})Fe^{III}(OH)$ [possibly in equilibrium with a minor fraction of the six-coordinate $(P^{8-})Fe^{III}(OH)(H_2O)$ species]. It is concluded on the basis of the UV−vis, ^1H NMR, and ^{17}O NMR data reported above that the studied porphyrin complex exists as **1-H_2O** in the pH 5−8 range and forms the monomeric monohydroxo species $(P^{8-})Fe^{III}(OH)$ as a predominant porphyrin form at pH >9. No evidence for the formation of a dihydroxo species, $(P^{8-})Fe(OH)_2$, or μ-oxo-bridged dimers was obtained in the studied pH range, i.e., pH <13.

As can be seen from data summarized in Table 1, the pK_{a1} determined for **1-H_2O** is higher than the reported pK_{a1} values characterizing deprotonation of a water molecule in other water-soluble $(P)Fe^{III}(H_2O)_2$ porphyrins. Such a high pK_{a1} apparently reflects the electronic effects of the negatively charged meso substituents that increase the electron density on the metal center (and thus disfavor the release of a proton from coordinated water), as well as through-space interactions of $RCOO^-$ groups with the axially coordinated water molecules. In the latter case, the formation of hydrogen bonds with deprotonated carboxylate groups of flexible malonate substituents (compare Figure S1 in the Supporting Information) is expected to stabilize coordinated water and the local 1+ charge of the $[Fe^{III}(N_p)_4]^+$ unit, thus increasing the pK_{a1} value. A similar influence of through-space interactions with negatively charged SO_3^- groups increasing the pK_{a1} value of coordinated water has been reported for another negatively charged water-soluble ferric porphyrin, viz., $(TanP^{4-})Fe^{III}(H_2O)_2$.[7a]

An interesting observation that can be added on the basis of the data reported in Tables 1 and 2 is that the lability of water coordinated to the iron(III) center apparently correlates with the contribution of the intermediate $S = {}^3/_2$ spin state in the admixed $S = {}^5/_2$, ${}^3/_2$ spin system of $(P)Fe^{III}(H_2O)_2$ complexes. This contribution can be estimated for iron(III) complexes of *meso*-tetraarylporphyrins on the basis of the β-pyrrole proton chemical shift (δ) according to eq 7.[19] The

$$\text{Int } \% = [(80 - \delta)/140] \times 100\ (\%) \qquad (7)$$

Int % values calculated from eq 7 for water-soluble porphyrins reported in Table 2 clearly show that an increasing contribution of the $S = {}^3/_2$ state correlates with an increasing labilization of the axial water molecules, as indicated by higher rates of water exchange observed for these complexes. Taking into account that the strong tetragonal distortion resulting in long axial bonds is the representative feature of the $S = {}^3/_2$ spin state in iron(III) porphyrins, the increasing lability of axial H_2O apparently reflects the lengthening of the $Fe-OH_2$ bond in spin-admixed $S = {}^5/_2$, ${}^3/_2$ porphyrins with increasing contribution of the $S = {}^3/_2$ spin state. It has been shown that population of the $S = {}^3/_2$ spin state results from destabilization of the $d_{x^2-y^2}$ orbital; i.e., as the energy of the $d_{x^2-y^2}$ orbital increases, the ground state in iron(III) porphyrins with weak field ligands (such as H_2O) changes from mainly $S = {}^5/_2$ to mainly $S = {}^3/_2$. Hence, the larger contribution of the $S = {}^3/_2$ state in negatively charged porphyrins, in comparison to that observed for $(P^{n+})Fe(H_2O)_2$, apparently reflects destabilization of the $d_{x^2-y^2}$ orbital by repulsive interactions with the increased electron density on the pyrrole nitrogens. A similar effect has been reported for water-insoluble ferric porphyrins with meso substituents of varying electron-releasing ability.[16] It can be expected that the trend of increasing lability of axial positions observed for water-soluble porphyrins included in Table 2 will also be reflected in their reactivity toward NO. In fact, a correlation of the $S = {}^3/_2$ spin admixture and the rates of NO binding exists for diaqua-ligated $(P)Fe^{III}(H_2O)_2$, as discussed in detail in the following section.

Reactivity of 1-H_2O toward NO. The addition of NO gas to a deoxygenated solution of **1-H_2O** at pH <9 resulted in the spectral changes presented in Figure 4. The decrease in the absorbance at 400 nm accompanied by the appearance of new bands at 427 (Soret, $\epsilon = 1.5 \times 10^5$ M^{-1} cm^{-1}) and 540 nm indicates the formation of a typical low-spin iron(III) porphinatonitrosyl complex[4,6] in which the formal charge distribution can be described as $(P^{8-})Fe^{II}(NO^+)(H_2O)$ (eq 8).

$$(P^{8-})Fe^{III}(H_2O)_2 + NO \underset{k_{off}}{\overset{k_{on}}{\rightleftharpoons}} (P^{8-})Fe^{II}(NO^+)(H_2O) + H_2O$$
$$K_{NO} = k_{on}/k_{off} \qquad (8)$$

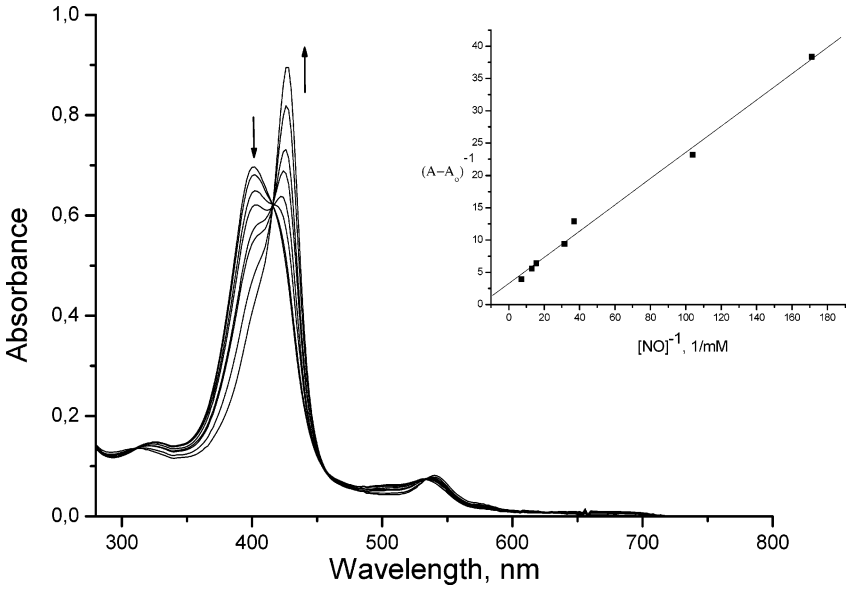

Figure 4. Spectral changes resulting from NO binding to $(P^{8-})Fe^{III}(H_2O)_2$. Inset: plot of $(A - A_0)^{-1}$ versus $[NO]^{-1}$ (where A_0 = absorbance at 400 nm at [NO] = 0, A = absorbance at 400 nm at a given NO concentration[10]). Experimental conditions: pH = 7 (0.05 M Bis-Tris), I = 0.1 M ($NaClO_4$), 22 °C.

Bubbling of an inert gas through the resulting solution leads to reversed spectral changes indicating reversibility of the reaction, in agreement with eq 8. The combination of UV−vis spectroscopy and amperometric detection of free NO in solution allowed the determination of the thermodynamic equilibrium constant $K_{NO} = (1.5 \pm 0.2) \times 10^4\ M^{-1}$ (compare the inset in Figure 4).

The kinetics of the reversible binding of NO to **1-H_2O** at pH 7 was studied by laser flash photolysis and stopped-flow techniques for the "on" and "off" reactions, respectively. Laser flash photolysis of $(P^{8-})Fe^{II}(NO^+)(H_2O)$ solutions resulted in transient spectral changes consistent with the spectral difference between $(P^{8-})Fe^{II}(NO^+)(H_2O)$ and $(P^{8-})Fe^{III}(H_2O)_2$. In the presence of excess NO, the transient spectrum decayed exponentially to the initial one. Thus, the processes occurring in the laser flash experiment can be summarized as follows.

$$H_2O + (P^{8-})Fe^{II}(NO^+)(H_2O) \underset{k_{off}}{\overset{h\nu,\ k_{on}}{\rightleftharpoons}} (P^{8-})Fe^{III}(H_2O)_2 + NO \quad (9)$$

The kinetics of the reaction was followed under pseudo-first-order conditions with at least a 10-fold excess of NO. As can be expected for the reversible process (eq 9), the k_{obs} values determined under such conditions by fitting the kinetic traces to a single-exponential function depend linearly on [NO] according to eq 10 (see Figure 5a). A linear fit of

$$k_{obs} = k_{on}[NO] + k_{off} \quad (10)$$

k_{obs} versus [NO] obtained at 24 °C allowed the determination of $k_{on} = (8.2 \pm 0.1) \times 10^5\ M^{-1}\ s^{-1}$ and $k_{off} = 217 \pm 16\ s^{-1}$ from the slope and intercept, respectively. The overall equilibrium constant calculated from the kinetic data, $K_{NO} = k_{on}/k_{off} = (3.8 \pm 0.2) \times 10^3\ M^{-1}$ (24 °C), is in reasonable agreement with the corresponding thermodynamic value of K_{eq} determined from a combination of UV−vis and electrochemical measurements. To determine the activation parameters $\Delta S^{\ddagger}$, $\Delta H^{\ddagger}$, and $\Delta V^{\ddagger}$ for the binding and release of NO, the kinetics was studied at different temperatures (6−30 °C) and hydrostatic pressures (0.1−170 MPa). The k_{on} and k_{off} values determined from linear dependences of k_{obs} versus [NO] at each temperature and pressure allowed the construction of Eyring plots for the "on" and "off" reactions (compare Figure 5) and a linear plot of $\ln(k_{on})$ versus pressure (Figure 6). Activation parameters calculated from the plots are summarized in Table 3. Because of the small intercepts in the plots of k_{obs} vs [NO] in the pressure-dependent study, the activation volume for the "off" reaction could not be determined accurately in this way. This value, however, could be measured in a stopped-flow experiment using the NO-trapping method. Rapid mixing of a $(P^{8-})Fe^{II}(NO^+)(H_2O)$ solution with a large excess of $[Ru(edta)(H_2O)]^-$ (an efficient scavenger for NO)[46] led to re-formation of the $(P^{8-})Fe^{III}(H_2O)_2$ complex, as indicated by the observed spectral change. The kinetics of the reaction was followed at 427 nm. The kinetic traces gave good mathematical fits to a single-exponential function, and the observed reaction rates did not depend on $[Ru(edta)(H_2O)^-]$ in the concentration range used in the NO-trapping experiments (1−2 mM). These observations indicate that the release of NO from $(P^{8-})Fe^{II}(NO^+)(H_2O)$ follows the reaction sequence in Scheme 1, in which k_{off} is the rate-determining step, such that the k_{obs} values determined from the kinetic traces equal k_{off}.

As can be seen from the data in Table 3, the rate constants obtained from variable-temperature NO-trapping measurements are in reasonable agreement with those resulting from the laser flash photolysis experiments. Small deviations of the k_{off} values obtained by these two techniques were, however, observed, particularly at higher temperatures (a similar tendency was also observed in measurements at pH 11; see further text). This presumably reflects a diminished

(46) Wanat, A.; Schneppensieper, T.; Karocki, A.; Stochel, G.; van Eldik, R. *J. Chem. Soc., Dalton Trans.* **2002**, 941.

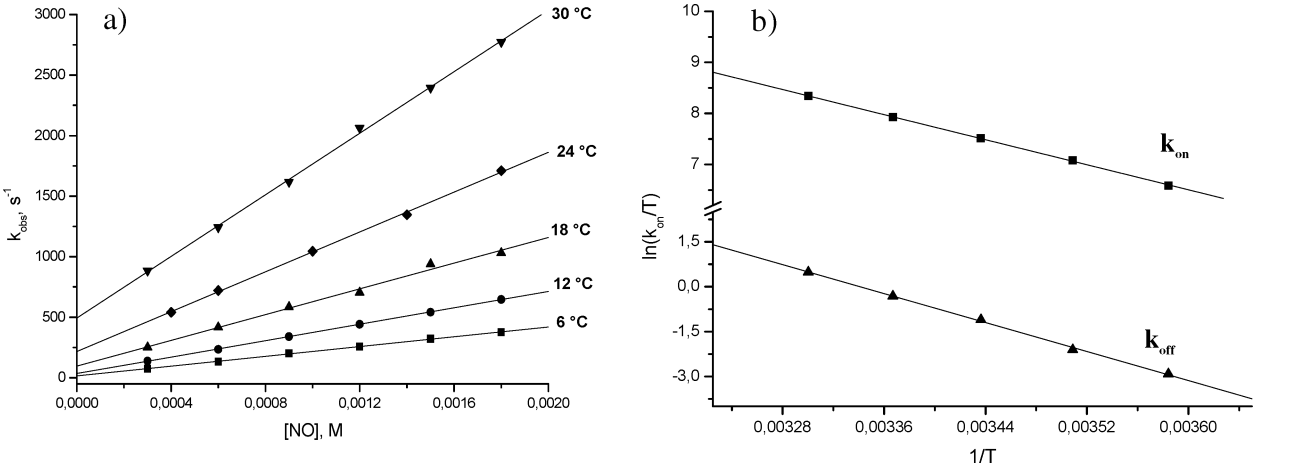

Figure 5. (a) Plots of k_{obs} versus [NO] for the reaction of **1-H_2O** with nitric oxide in the temperature range 6−30 °C measured by laser flash photolysis. (b) Corresponding Eyring plots for the "on" and "off" reactions. Experimental conditions: [**1-H_2O**] = 2.0×10^{-5} M, pH 7 (0.05 M Bis-Tris), λ_{irr} = 355 nm, λ_{det} = 417 nm, I = 0.1 M ($NaClO_4$).

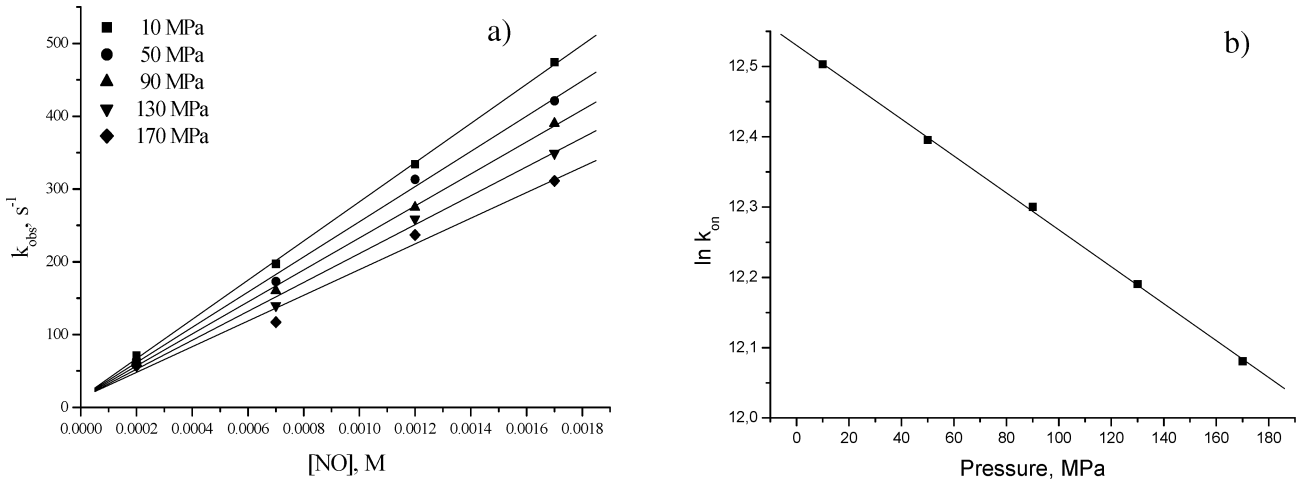

Figure 6. (a) Plots of k_{obs} versus [NO] for the reaction of **1-H_2O** with NO in the pressure range of 10−170 MPa. (b) Plot of ln(k_{on}) versus pressure. Experimental conditions: [**1-H_2O**] = 2.0×10^{-5} M, pH 7 (Bis-Tris, 0.05 M), λ_{irr} = 355 nm, λ_{det} = 417 nm, I = 0.1 M ($NaClO_4$).

efficiency of $[Ru^{III}(edta)(H_2O)]^-$ as the NO trap at pH >6 because of its deprotonation to a less reactive $[Ru^{III}(edta)(OH)]^{2-}$ form.[46] Nevertheless, the similarity of the activation parameters $\Delta H^{\ddagger}_{off}$ and $\Delta S^{\ddagger}_{off}$ determined from laser flash photolysis and NO-trapping studies (Table 3) indicates that the NO-trapping method provides a reliable mechanistic description of the "off" reaction at pH 7. This technique was therefore used to determine $\Delta V^{\ddagger}$ for the "off" reaction. The stopped-flow NO-trapping measurements performed in the pressure range of 0.1−130 MPa allowed the determination of $\Delta V^{\ddagger}_{off} = +16.8 \pm 0.4$ cm^3 mol^{-1}.[47]

A comparison of the rate and activation parameters for the binding and release of NO obtained for **1-H_2O** with those reported in the literature for other water-soluble ferric porphyrins (compare Table 4) shows that the reactivity of the diaqa-ligated **1-H_2O** toward NO is similar to that observed for other $(P^{n-})Fe(H_2O)_2$ complexes. Although the "on" and "off" rate constants reported for $(TMPyP^{4+})Fe^{III}(H_2O)_2$ with positively charged meso substituents are markedly smaller in comparison to those observed for $(P^{n-})Fe(H_2O)_2$, the similarity of the activation parameters (in

Table 3. Rate Constants and Activation Parameters Determined by Laser Flash Photolysis and Stopped-Flow (NO-Trapping Method) Techniques for the Reversible Binding of NO to $(P^{8-})Fe^{III}(H_2O)_2$ at pH 7

temp (°C)	pressure (MPa)	$k_{on} \times 10^{-5}$ (M^{-1} s^{-1})	k_{off} (s^{-1})	k_{off}[a] (s^{-1})
6		2.0 ± 0.1	15 ± 1	10.5 ± 0.5
10				23.0 ± 0.5
12		3.4 ± 0.1	34 ± 2	31.0 ± 0.4
18		5.3 ± 0.2	96 ± 28	81 ± 2
24		8.2 ± 0.1	217 ± 16	220 ± 2
30		12.7 ± 0.1	494 ± 24	432 ± 12
10	10	2.7 ± 0.1	8.4 ± 0.2[b]	
	50	2.4 ± 0.1	6.7 ± 0.1[b]	
	90	2.2 ± 0.1	4.8 ± 0.3[b]	
	130	1.9 ± 0.1	3.5 ± 0.2[b]	
	170	1.7 ± 0.1		
$\Delta H^{\ddagger}$ (kJ mol^{-1})		51.1 ± 0.5	101 ± 2	107 ± 3
$\Delta S^{\ddagger}$, (J mol^{-1} K^{-1})		+40 ± 2	+140 ± 7	+160 ± 10
$\Delta V^{\ddagger}$ (cm^3 mol^{-1})		+6.1 ± 0.1		+16.8 ± 0.4

[a] Data obtained by the NO-trapping method using $[Ru^{III}(edta)(H_2O)]^-$ (unbuffered solution, pH 7). [b] Data obtained by the NO-trapping method at 3 °C.

(47) Plots of ln(k_{off}/T) versus 1/T and ln(k_{off}) versus pressure constructed from data obtained in the NO-trapping experiments are shown in Figure S4 in the Supporting Information.

Scheme 1

$$(P^{8-})Fe^{II}(NO^{+})(H_2O) + H_2O \underset{k_{on}}{\overset{k_{off}}{\rightleftharpoons}} (P^{8-})Fe^{III}(H_2O)_2 + NO$$

$$(P^{8-})Fe^{III}(H_2O)_2 + NO \xrightarrow{\text{fast}} [Ru^{III}(edta)(H_2O)]^{-}$$

$$[Ru^{III}(edta)(NO)]^{-} + H_2O$$

Table 4. Comparison of Rate Constants and Activation Parameters for Binding and Release of NO for Water-Soluble Diaqua-Ligated Iron(III) Porphyrins

iron(III) porphyrin	Int %	k at 25 °C	$\Delta H^{\ddagger}$ (kJ mol^{-1})	$\Delta S^{\ddagger}$ (J mol^{-1} K^{-1})	$\Delta V^{\ddagger}$ (cm^3 mol^{-1})
			k_{on} (M^{-1} s^{-1})		
1-H_2O	24	8.2×10^5	51 ± 1	$+40 \pm 2$	$+6.1 \pm 0.1$
$(TMPS^{4-})Fe(H_2O)_2$[a]	26	3.8×10^6	57 ± 3	$+69 \pm 11$	$+13 \pm 1$
$(TPPS^{4-})Fe(H_2O)_2$[a]	20	5×10^5	69 ± 3	$+95 \pm 10$	$+9 \pm 1$
$(TMPyP^{4+})Fe(H_2O)_2$[b]	7	2.9×10^4	67 ± 3	$+67 \pm 11$	$+3.9 \pm 1.0$
			k_{off} (s^{-1})		
1-H_2O	24	217	101 ± 2	$+140 \pm 7$	$+16.8 \pm 0.4$
$(TMPS^{4-})Fe(H_2O)_2$[a]	26	900	84 ± 3	$+94 \pm 10$	$+17 \pm 3$
$(TPPS^{4-})Fe(H_2O)_2$[a]	20	500	76 ± 6	$+60 \pm 11$	$+18 \pm 2$
$(TMPyP^{4+})Fe(H_2O)_2$[b]	7	66	113 ± 5	$+169 \pm 18$	$+16.6 \pm 0.2$

[a] Data from ref 4. [b] Data from ref 6.

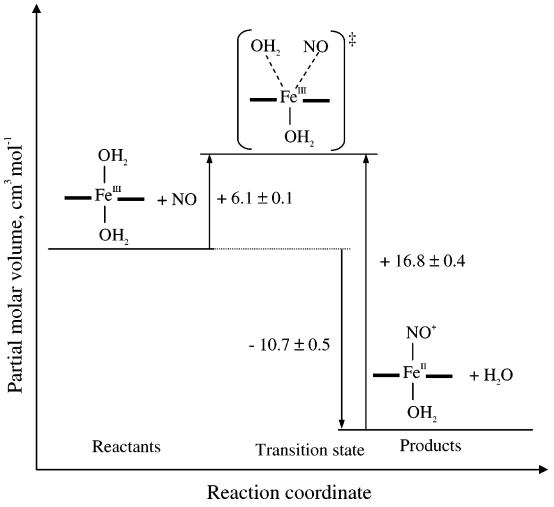

Figure 7. Volume profile for the reversible binding of nitric oxide to $(P^{8-})Fe^{III}(H_2O)_2$.

particular, $\Delta S^{\ddagger}$ and $\Delta V^{\ddagger}$) shows that the mechanistic features of the binding and release of NO are analogous for both positively and negatively charged $(P)Fe^{III}(H_2O)_2$ species. Thus, the volume profile constructed from the activation volumes, $\Delta V^{\ddagger}_{on}$ and $\Delta V^{\ddagger}_{off}$, obtained for **1-$H_2O$** (Figure 7) reflects a common reaction mechanism for the diaqua forms of water-soluble porphyrins, in which the "on" reaction is controlled by substitution of a water molecule according to a dissociative (I_d or D)[48] mechanism, as evidenced by the positive values of $\Delta V^{\ddagger}_{on}$.[4,6] The rate-determining substitution step is followed by a large volume collapse due to a spin-state change and solvent reorganization accompanying the formation of the low-spin $(P)Fe^{II}(NO^{+})(H_2O)$ product. The large positive volumes of activation typical for the "off" reaction clearly indicate that the release of NO also follows a dissociative mechanism. The rate-determining breakage of the $Fe^{II}-NO^{+}$ bond (resulting in a positive contribution to $\Delta V^{\ddagger}_{off}$) is in this case accompanied by a further volume increase due to formal oxidation ($Fe^{II} \rightarrow Fe^{III}$) and spin-state change ($S = 0 \rightarrow S = {}^5/_2, {}^3/_2$) on the iron(III) center, as well as solvent reorganization due to neutralization of the partial charge on the $Fe^{II}-NO^{+}$ unit.

It can also be seen from the data in Table 4 that the increase in the rate of NO binding correlates directly with the rising contribution of the intermediate $S = {}^3/_2$ spin state (Int %) in the admixed $S = {}^5/_2, {}^3/_2$ spin system of the $(P)Fe^{III}(H_2O)_2$ complexes, as previously observed for the water-exchange rates. This provides additional evidence that the lability of the axial water controls to a large extent the kinetics of NO binding. It can be further concluded from data in Table 4 that the rate of NO release from a $(P)Fe^{II}(NO^{+})(H_2O)$ complex tends to increase with increasing electron-donating influence of *meso*-porphyrin substituents [reflected by the rising contribution of $S = {}^3/_2$ in the spin-admixed state of $(P)Fe^{III}(H_2O)_2$]. Although the correlation of k_{off} and Int % is not as clear as in the case of the NO-binding rates, it suggests that the $Fe^{II}-NO^{+}$ bond in $(P)Fe^{II}(NO^{+})(H_2O)$ is better stabilized by the positively charged porphyrins than by the negatively charged ones. This is in line with recent literature reports that, based on resonance Raman and density functional theory (DFT) results, indicate that a gradual increase of the electron density within the Fe−NO unit induced by meso substituents destabilizes the Fe−NO bond in the porphyrin $\{FeNO\}^6$ nitrosyls.[49]

Reactivity of Monohydroxo-Ligated $(P^{8-})Fe(OH)$ (1-OH) toward NO. Spectroscopic and kinetic studies on the reaction of **1** with NO performed at pH >9 indicated differences in the kinetics of NO binding and release, as well as in the nature of the nitrosyl species formed at high pH in comparison to that observed at pH <9. The spectral changes

(48) (a) Helm, L.; Merbach, A. E. *Chem. Rev.* **2005**, *105*, 1923. (b) Richens, D. T. *Chem. Rev.* **2005**, *105*, 1961.

(49) (a) Linder, D. P.; Rodgers, K. R.; Banister, J.; Wyllie, G. R. A.; Ellison, M. K.; Scheidt, W. R. *J. Am. Chem.* Soc. **2004**, *126*, 14136. (b) Linder, D. P.; Rodgers, K. R. *J. Am. Chem. Soc.* **2005**, *44*, 1367.

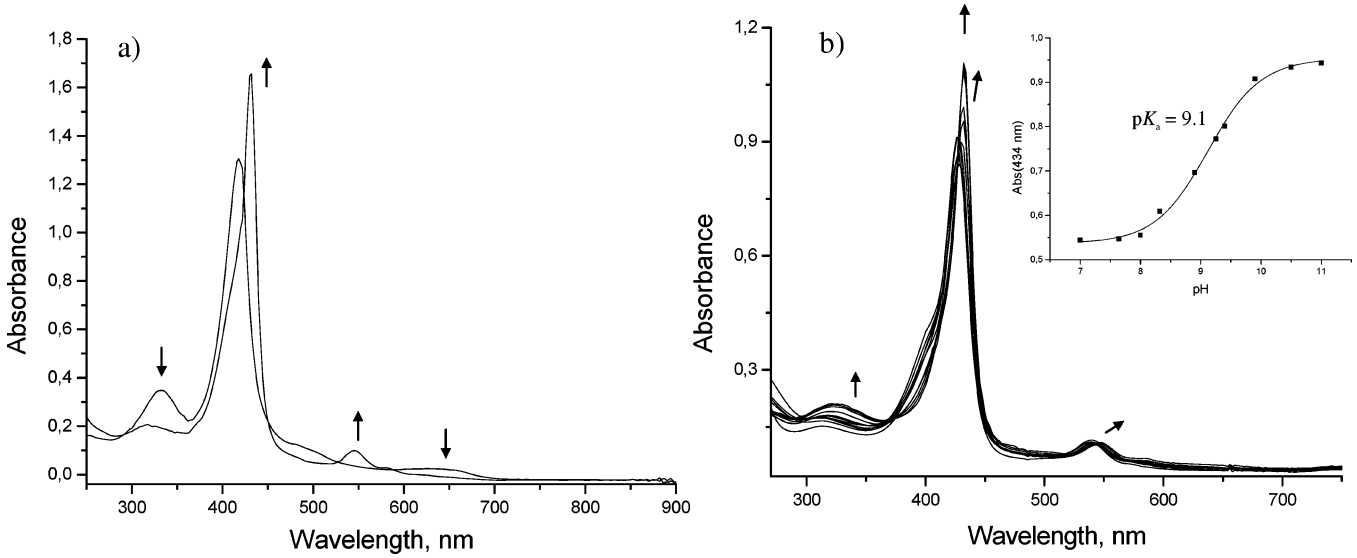

Figure 8. (a) Spectral change accompanying the reaction of **1-OH** with NO at pH 11. (b) Spectra of the product obtained in the reaction of **1** with NO in buffered aqueous solutions in the pH 7−11 range. A plot of ΔAbs_{434} versus pH is shown in the inset. Experimental conditions: [**1**] $\approx 7 \times 10^{-6}$ M, [NO] = 1 mM, $I = 0.1$ M ($NaClO_4$). Buffers used: pH 7, Bis-Tris (0.05 M); pH 7.5−8.8, TAPS (0.05 M); pH 9.1, borate (0.05 M); pH 9.5−11, CAPS (0.05 M).

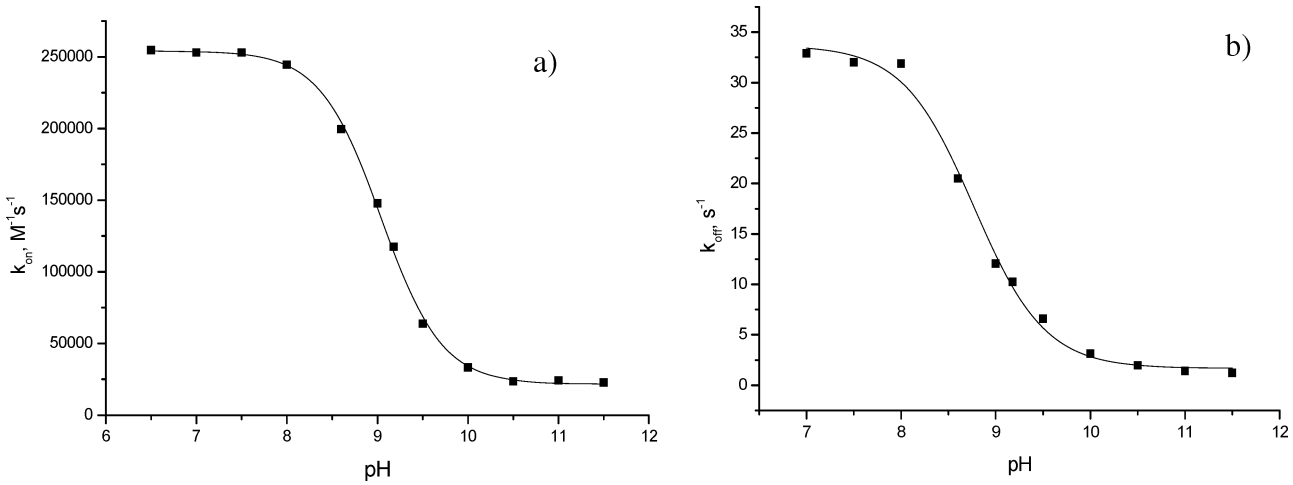

Figure 9. pH dependence of the rate constants for binding (a) and release (b) of NO from **1** determined from the slopes and intercepts of k_{obs} versus [NO] plots measured in buffered aqueous solutions in the pH 6.5−11.5 range. Experimental conditions: [**1**] $= 2.0 \times 10^{-5}$ M, 10 °C, $I = 0.1$ M ($NaClO_4$).

that accompany the reaction of **1-OH** with NO at pH 11 (Figure 8a) lead to a final spectrum in which the characteristic peaks at 317, 432 (Soret, $\epsilon = 1.9 \times 10^5$ M^{-1} cm^{-1}), and 544 nm occur at longer wavelengths as compared to those observed at lower pH (viz., 310, 427, and 540 nm). The spectral changes reported in Figure 8b show a gradual change in the spectrum of the nitrosyl product obtained by the reaction of the ferric porphyrin with NO in buffered aqueous solutions as a function of pH in the range 7−11. A fit of the plot of ΔAbs_{434} vs pH (inset in Figure 8b) allowed the determination of $pK_{a(NO)} = 9.1$ for the pH-dependent equilibrium associated with the observed spectral change. This equilibrium is ascribed to deprotonation of a coordinated water molecule in $(P^{8-})Fe^{II}(NO^+)(H_2O)$ according to eq 11.

$$(P^{8-})Fe^{II}(NO^+)(H_2O) \rightleftarrows (P^{8-})Fe^{II}(NO^+)(OH) + H^+ \qquad pK_{a(NO)} = 9.1 \quad (11)$$

Combined UV−vis and NO electrode measurements allowed the determination of equilibrium constant $K_{NO} = (4.8 \pm 0.5) \times 10^3$ M^{-1} for the reversible binding of NO to **1-OH** at pH 11. This value is similar to that derived kinetically from the rate constants $k_{on} = 5.1 \times 10^4$ M^{-1} s^{-1} and $k_{off} = 14.9$ s^{-1} (24 °C) determined from the dependence of k_{obs} on [NO] at pH 11, viz., $K_{NO} = k_{on}/k_{off} = (3.4 \pm 0.1) \times 10^3$ M^{-1}. A comparison of k_{on} and k_{off} measured at pH 11 with those obtained at pH 7 ($k_{on} = 8.2 \times 10^5$ M^{-1} s^{-1} and $k_{off} = 217$ s^{-1}) shows that both coordination and release of NO decreases ca. 15 times at high pH. Figure 9 presents the pH dependence of k_{on} and k_{off} values determined from k_{obs} versus [NO] plots in the pH 6.5−11.5 range. It can be seen from these data that the rates of NO binding and dissociation gradually decrease between pH 7.5 and 10.5 and become constant at pH >11. The pK_a value determined by fitting the data in Figure 9a to a sigmoidal function, viz., 9.04 ± 0.01, is close to the $pK_{a1} = 9.26$ determined from a spectrophotometric titration of **1**, which characterizes deprotonation of a water molecule in **1-H_2O** (eq 6). This indicates that the change in reactivity observed on increasing pH

Scheme 2

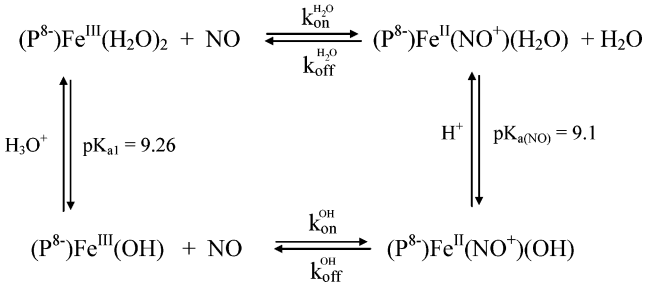

reflects differences in the kinetics of NO binding to **1-H_2O** and **1-OH** present in solution at low and high pH, respectively. An analogous sigmoidal fit of the less precise data in Figure 9b (constructed on the basis of k_{off} values obtained by extrapolation of k_{obs} versus [NO] plots to [NO] = 0) resulted in pK_a = 8.9 ± 0.1, which is also close to that characteristic for the formation of the hydroxo-ligated porphyrin (eq 6), as well as that estimated for the process depicted in eq 11 (p$K_{a(NO)}$ = 9.1). It is apparent from these data that the presence of the hydroxo group decreases the rate of NO binding to $(P^{8-})Fe^{III}$, as well as the rate of NO release from $(P^{8-})Fe^{II}(NO^+)(OH)$. The observed reactivity pattern is summarized in Scheme 2, in which the rate constants for **1-H_2O** and **1-OH** species are denoted by k^{H_2O} and k^{OH}, respectively.

The observation that the rate of NO binding to $(P^{8-})Fe^{III}$ *decreases* on going from a *trans*-diaqua to an hydroxo complex is surprising in view of kinetic data on the substitution behavior of such metal complexes in solution, where in the majority of cases an increase in the reactivity of the hydroxo form is observed as compared to the diaqua species. Such a trend reflects the significant labilizing influence of the hydroxo group, which facilitates substitution of the ligand coordinated in the trans position to OH^-.[50] The reversed reactivity pattern observed for **1-OH** indicates that binding of NO to **1-OH** is no longer controlled by the lability of the metal center (where, in such a case, a very fast diffusion-controlled rate for NO coordination to this five-coordinate iron(III) complex would be expected). Apparently, other factors determine the rate of formation of the nitrosylated species at high pH. This conclusion is further substantiated by a detailed study of the reversible binding of NO to **1-OH** at pH 11. Figures 10, S5, and S6 (in the Supporting Information) and Table 5 report the results of stopped-flow experiments performed at different temperatures and pressures for the reaction of **1-OH** with NO at pH 11. As can be seen from the data summarized in Table 5, the activation parameters determined for NO binding to **1-OH**, viz., $\Delta H^{\ddagger}_{on}$ = 34.6 kJ mol^{-1}, $\Delta S^{\ddagger}_{on}$ = −39 J mol^{-1} K^{-1}, and $\Delta V^{\ddagger}_{on}$ = −6.1 cm^3 mol^{-1}, are very different from that characterizing NO binding to the diaqua forms of water-soluble porphyrins given in Table 4. In particular, negative values of $\Delta S^{\ddagger}_{on}$ and $\Delta V^{\ddagger}_{on}$ contrast the positive ones observed at low pH and indicate a changeover in the mechanism of NO binding from dissociatively activated (I_d) in **1-H_2O** to associatively activated in **1-OH**. This difference is particularly evident on comparing the volume profile in Figure 7 with that constructed for the reversible binding of NO to $(P^{8-})Fe^{III}(OH)$, as shown in Figure 11. Notably, the latter profile is very similar to that reported in the literature for reversible binding of NO to the high-spin five-coordinate (P)Fe^{III}(Cys) center in substrate-bound Cytochrome $P450_{cam}$.[9a] The activation volumes $\Delta V^{\ddagger}_{on}$ = −7.3 cm^3 mol^{-1} and $\Delta V^{\ddagger}_{off}$ = +24 cm^3 mol^{-1} determined for this ferric protein were interpreted in terms of the mechanistic scheme outlined in eq 12, in which rapid formation of an encounter complex,

$$(P)Fe^{III}(Cys) + NO \underset{k_{-D}}{\overset{k_D}{\rightleftharpoons}} \{(P)Fe^{III}(Cys)||NO\} \xrightarrow{k_a} (P)Fe^{II}(Cys)(NO^+) \quad (12)$$

$\{(P)Fe^{III}||NO\}$, is followed by the activation step involving the formation of the Fe−NO bond.[9a]

In the above scheme, k_D and k_{-D} represent the rate constants for the diffusion-limited formation and dissociation of the encounter complex and k_a is the rate constant for Fe−NO bond formation. The relatively small negative value of $\Delta V^{\ddagger}_{on}$ = −7.3 cm^3 mol^{-1} observed for Cyt $P450_{cam}$ was ascribed to an activation-controlled mechanism with an "early" transition state, in which only partial (P)Fe^{III}−NO bond formation and a change in the spin state of the Fe^{III} center ($S = {}^5/_2 \rightarrow S = 0$) occurs on going from the encounter complex to the transition state $\{(P)Fe^{III}\text{- - -}NO\}^{\ddagger}$. A large positive $\Delta V^{\ddagger}_{off}$ value of 24 cm^3 mol^{-1} observed for the backward reaction evidenced a subsequent large volume collapse on going from the transition state to the low-spin (P)$Fe^{II}(NO^+)$ product. The data obtained in the present study for $(P^{8-})Fe^{III}(OH)$ strongly suggest an analogous reaction mechanism, as summarized in Scheme 3. According to this scheme, initial partial formation of the Fe−NO bond in the transition state (accounting for the negative $\Delta V^{\ddagger}_{on}$ = −6.1 cm^3 mol^{-1}) is followed by volume collapse (ca. 17 cm^3 mol^{-1}) due to complete formation of the Fe^{II}−NO^+ bond, $S = {}^5/_2 \rightarrow S = 0$ spin change, and solvent contraction accompanying partial charge transfer from NO to Fe^{III}.

The mechanistic difference observed in the binding of NO to **1-H_2O** and **1-OH** is further reflected in the k_{on} values observed for the diaqua- and hydroxo-ligated species, respectively. The ca. 15-fold decrease in the rate of NO binding to the five-coordinate (or weakly six-coordinate) hydroxo form implies that the formation of $(P^{8-})Fe^{II}(NO^+)$-(OH) is not controlled by the lability of the Fe^{III} center but rather by the enthalpy and entropy changes associated with spin reorganization and structural rearrangements upon the formation of the Fe^{II}−NO^+ bond. This situation parallels that previously observed in the reactions of five-coordinate Fe(II) hemes with CO, for which an analogous mechanistic scheme was suggested. In these earlier studies,[4] considerably slower rates of CO coordination to (P)Fe^{II} as compared to NO binding rates determined for the same complexes (which approached the diffusion limit in water) and an associative-activated mechanism were interpreted in terms of a significant activation barrier associated with spin state/structural

(50) Cusanelli, A.; Frey, U.; Ritchens, D. T.; Merbach, A. E. *J. Am. Chem. Soc.* **1996**, *118*, 5265 and references cited therein.

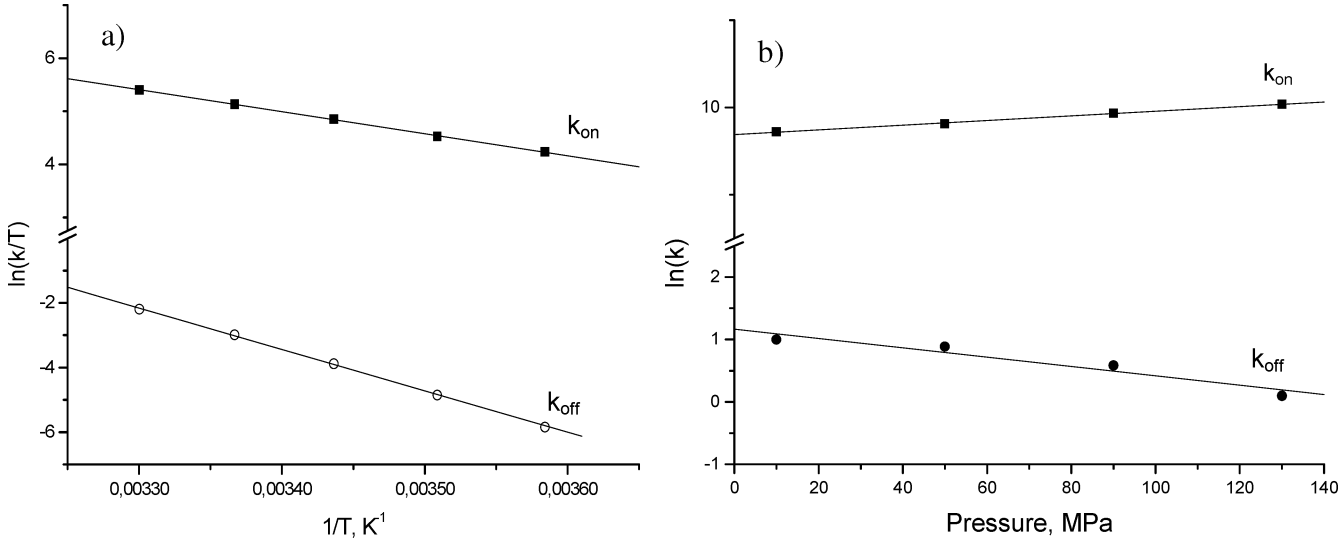

Figure 10. (a) Eyring plots of ln(k/T) versus 1/T obtained for the "on" and "off" reactions in stopped-flow variable-temperature studies on reversible binding of NO to **1-OH**. Experimental conditions: [**1-OH**] = 2.0×10^{-5} M, pH 11 (0.05 M CAPS buffer), I = 0.1 M ($NaClO_4$), λ_{det} = 432 nm. (b) Plots of ln(k) versus pressure determined for the same reaction by high-pressure stopped-flow measurements in the pressure range of 10−130 MPa. Experimental conditions: [**1-OH**] = 1.2×10^{-5} M, pH 11 (0.05 M CAPS buffer), I = 0.1 M ($NaClO_4$), λ_{det} = 430 nm, 1.5 °C.

Table 5. Rate Constants and Activation Parameters for Binding and Release of NO from $(P^{8-})Fe^{III}(OH)$ at pH 11

temp (°C)	pressure (MPa)	$k_{on} \times 10^{-4}$ ($M^{-1}\,s^{-1}$)	k_{off}[a] (s^{-1})	k_{off}[b,c] (s^{-1})
6		1.9 ± 0.1	0.70 ± 0.02	0.86 ± 0.01
12		2.6 ± 0.1	2.2 ± 0.3	1.97 ± 0.02
18		3.7 ± 0.1	6.0 ± 0.5	5.1 ± 0.1
24		5.1 ± 0.2	14.9 ± 0.3	11.4 ± 0.3
30		6.7 ± 0.1	33.9 ± 0.7	23.7 ± 0.3
1.5	10	1.67 ± 0.06	2.7 ± 0.3	0.16 ± 0.01[d]
	50	1.83 ± 0.03	2.4 ± 0.2	0.12 ± 0.01[d]
	90	2.06 ± 0.02	1.8 ± 0.1	0.09 ± 0.01[d]
	130	2.29 ± 0.05	1.1 ± 0.3	0.06 ± 0.01[d]
$\Delta H^{\ddagger}$ (kJ mol^{-1})		34.6 ± 0.4	107 ± 2	96 ± 1[c]
$\Delta S^{\ddagger}$ (J $mol^{-1}\,K^{-1}$)		−39 ± 1	+136 ± 7	+97 ± 4[c]
$\Delta V^{\ddagger}$ ($cm^3\,mol^{-1}$)		−6.1 ± 0.2	+17 ± 3	+21.3 ± 0.4[c]

[a] Data obtained from intercepts of plots of k_{obs} versus [NO]. [b] Data obtained with the use of $[Ru^{III}(edta)(H_2O)]^-$ as the NO scavenger. [c] Systematic deviations of the k_{off} values from those determined as intercepts of k_{obs} versus [NO] plots point to a low efficiency of NO trapping by Ru(edta) at pH 11. Therefore, the activation parameters obtained in alternative measurements (Figure 10) are preferentially used for mechanistic characterization of NO release at high pH. [d] Measured at 3 °C.

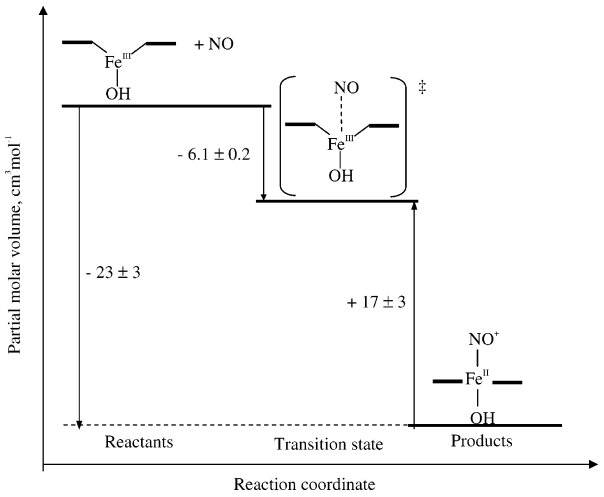

Figure 11. Volume profile for the reversible binding of nitric oxide to $(P^{8-})Fe^{III}(OH)$.

changes upon coordination of CO (which, however, was absent in the reactions with NO). This conclusion was further substantiated by recent DFT computations performed for the (P)Fe(II) + CO system.[51] The decrease in k_{on} observed in the present case for NO coordination to the Fe(III) porphyrin complex **1** at high pH is ascribed to a larger intrinsic activation barrier for the $S = {}^5/_2 \rightarrow S = 0$ spin state change, which occurs upon the formation of $(P^{8-})Fe^{II}(NO^+)(OH)$ from the purely high-spin hydroxo species **1-OH**, as compared to that associated with the ($S = {}^5/_2$, ${}^3/_2 \rightarrow S = 0$) spin change occurring for the diaqua-ligated spin-admixed **1-H_2O** complex. As pointed out in recent mechanistic studies on a spin-forbidden proton-transfer reaction in solution,[52] such an increased "intersystem barrier" can be related to a spin-forbidden transition itself and/or to a considerable structural reorganization required to enable the spin change. Consideration of characteristic structural features reported for five-coordinate high-spin, six-coordinate spin-admixed, and low-spin $(P)Fe^{III}(L)_n$ porphyrins, respectively, suggests that rather minor structural changes are required for the formation of low-spin $(P)Fe^{II}(NO^+)(H_2O)$ from spin-admixed **1-H_2O** species, where in both complexes the iron atom lies in the porphyrin plane, is six-coordinate, and exhibits short equatorial Fe−N_p bonds. In contrast, the binding of NO to **1-OH** presumably involves a change in the coordination number of the Fe(III) atom, its movement into the porphyrin plane, and contraction of the Fe−N_p equatorial bond; i.e., a considerable structural change (and thus higher energy barrier) is expected to occur upon going from the substrate to product.

An additional contribution to the observed decrease in k_{on} at high pH may arise from a difference in the reducibility of the Fe^{III} center in $(P)Fe^{III}(H_2O)_2$ and $(P)Fe^{III}(OH)$. As

(51) Harvey, J. N. *J. Am. Chem. Soc.* **2000**, *122*, 12401.
(52) Shafirovich, V.; Lymar, S. V. *J. Am. Chem. Soc.* **2003**, *125*, 6547.

Scheme 3

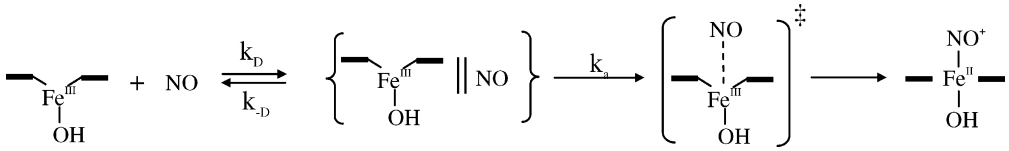

indicated by literature data, deprotonation of a water molecule in $(P)Fe^{III}(H_2O)_2$ species shifts the potentials of Fe^{III} reduction to more negative values in comparison to that observed for diaqua-ligated forms.[53,54] Because the formation of the $Fe^{III}-NO$ bond is accompanied by charge transfer from NO and formal reduction of the Fe^{III} center, a decrease in the rate of this process can be expected for less easily reducible hydroxo-ligated species in comparison to the $(P)Fe^{III}(H_2O)_2$ counterparts.

In view of the fact that the spin changes (and the accompanying structural changes) are clearly involved in the rate-determining step for the "off" reaction (i.e., breakage of the $Fe^{II}-NO^+$ bond) in both $(P^{8-})Fe^{II}(NO^+)(H_2O)$ and $(P^{8-})Fe^{II}(NO^+)(OH)$, it is suggested that the decreased reaction rate observed for the release of NO at high pH reflects a larger demand for reorganization of d electrons upon re-formation of **1-OH** from the corresponding nitrosyl complex (i.e., $S = 0 \rightarrow S = {}^5/_2$) in comparison to that occurring for $(P^{8-})Fe^{II}(NO^+)(H_2O)$ ($S = 0 \rightarrow S = {}^5/_2, {}^3/_2$).

Taken together, the kinetic and mechanistic data described above provide strong evidence that the rate of NO binding and release observed for hydroxo-ligated species is to a large extent controlled by the degree of spin reorganization occurring at the Fe^{III} center on going from reactants to products. Notably, the k_{on} and k_{off} rates determined in the present study for **1-OH** (viz., $k_{on} = 5.1 \times 10^4\ M^{-1}\ s^{-1}$ and $k_{off} = 14.9\ s^{-1}$ at 24 °C) are quite similar to those reported for the $(TMPyP^{4+})Fe(H_2O)_2$, which is almost purely high spin (Int % = 7%, $k_{on} = 2.9 \times 10^4\ M^{-1}\ s^{-1}$, $k_{off} = 66\ s^{-1}$ at 25 °C; compare Table 4), but considerably smaller than those observed for $(P^{n-})Fe(H_2O)_2$ species exhibiting a relatively large contribution of the $S = {}^3/_2$ spin state (ca. 26%), further supporting the above conclusion. The observations on the influence of the spin and ligation states of the Fe^{III} center on the dynamics of the reaction with NO are important to understand kinetic and mechanistic factors governing the interactions of NO with naturally occurring heme proteins, in which a variety of spin and ligation states are observed. This stimulated further in-depth mechanistic studies on the reversible binding of NO to model $(P)Fe^{III}(L)_n$ complexes with different types of porphyrin and axial ligands, which will be described in a subsequent report.

Conclusions

According to the data reported in this study, introduction of four flexible malonate substituents on the highly negatively charged iron(III) porphyrin **1** increases the pK_{a1} of coordinated water in **1-H$_2$O** to the highest value reported to date. This is ascribed to through-space interactions of negatively charged substituents with coordinated water, as well as to electronic effects. The latter effects are reflected in partial depopulation of the iron $d_{x^2-y^2}$ atomic orbital, leading to ca. 26% contribution of the $S = {}^3/_2$ spin state in the spin-admixed $(P^{8-})Fe^{III}(H_2O)_2$ system. This contribution is relatively high in comparison with those of other $(P)Fe^{III}(H_2O)_2$ species and correlates with the high lability of coordinated water, as is indicated by rapid water-exchange and NO coordination rates observed for the **1-H$_2$O** complex. The solution pH determines the nature of the axial ligands in **1** and thereby controls the coordination number, spin state, and reactivity of the iron(III) center toward NO. The predominantly five-coordinate, purely high-spin **1-OH** formed at pH >9 binds NO according to an associative mechanism, in contrast to a dissociatively activated process observed for six-coordinate **1-H$_2$O** at lower pH. In the case of **1-OH**, however, the NO binding step is no longer controlled by the lability of the metal center. Other (most probably electronic and structural) factors involved in the rate-limiting Fe−NO bond formation and breakage (for the "on" and "off" reactions, respectively) apparently account for the slower rate of NO binding and release observed at high pH for **1-OH**. Correlations between spin/ligation states and reactivity inferred on the basis of spectroscopic and kinetic data for other water-soluble iron(III) porphyrins studied to date further support this conclusion. As suggested by preliminary studies on other water-soluble iron(III) porphyrins, the pH-reactivity pattern reported here for water-exchange and reversible NO binding to **1** is a common phenomenon for diaqua- and monohydroxo-ligated $(P)Fe^{III}$ species in aqueous media. Because of the potential significance of this observation for studies on NO interactions with heme proteins (in which a variety of spin and ligation states are observed), the mechanistic conclusions inferred here will be supplemented and verified by further studies that will be reported in a subsequent paper.

Acknowledgment. The authors gratefully acknowledge financial support from the Deutsche Forschungsgemeinschaft within SFB 583 "Redox-active metal complexes", Fonds der Chemischen Industrie, and the DAAD/KGN exchange program.

Supporting Information Available: Figures S1−S7, Table S1, and X-ray crystallographic data for **2** (CIF format). This material is available free of charge via the Internet at http://pubs.acs.org.

IC050924T

(53) Batinic-Haberle, I.; Spasojevic, I.; Hambright, P.; Benov, L.; Crumbliss, A. L.; Fridovich, I. *Inorg. Chem.* **1999**, *38*, 4011.
(54) Liu, M.; Su, Y. O. *J. Electroanal. Chem.* **1998**, *452*, 113.